FOR OFFICIAL USE ONLY

JPRS L/8338

15 March 1979

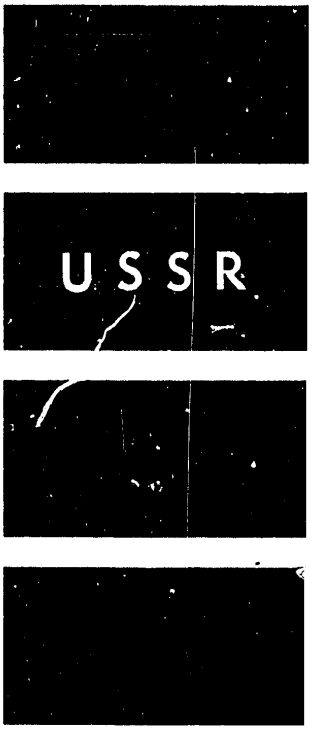

TRANSLATIONS ON USSR SCIENCE AND TECHNOLOGY
PHYSICAL SCIENCES AND TECHNOLOGY
(FOUO 15/79)

U. S. JOINT PUBLICATIONS RESEARCH SERVICE

FOR OFFICIAL USE ONLY

NOTE

JPRS publications contain information primarily from foreign newspapers, periodicals and books, but also from news agency transmissions and broadcasts. Materials from foreign-language sources are translated; those from English-language sources are transcribed or reprinted, with the original phrasing and other characteristics retained.

Headlines, editorial reports, and material enclosed in brackets [] are supplied by JPRS. Processing indicators such as [Text] or [Excerpt] in the first line of each item, or following the last line of a brief, indicate how the original information was processed. Where no processing indicator is given, the information was summarized or extracted.

Unfamiliar names rendered phonetically or transliterated are enclosed in parentheses. Words or names preceded by a question mark and enclosed in parentheses were not clear in the original but have been supplied as appropriate in context. Other unattributed parenthetical notes within the body of an item originate with the source. Times within items are as given by source.

The contents of this publication in no way represent the policies, views or attitudes of the U.S. Government.

APPROVED FOR RELEASE: 2007/02/08: CIA-RDP82-00850R000100030041-2

BIBLIOGRAPHIC DATA SHEET	1. Report No. JPRS L/ 8338	2.	3. Recipient's Accession No.
4. Title and Subtitle TRANSLATIONS ON USSR SCIENCE AND TECHNOLOGY - PHYSICAL SCIENCES AND TECHNOLOGY, (FOUO 15/79)			5. Report Date 15 March 1979 6.
7. Author(s)			8. Performing Organization Rept. No.
9. Performing Organization Name and Address Joint Publications Research Service 1000 North Glebe Road Arlington, Virginia 22201			10. Project/Task/Work Unit No. 11. Contract/Grant No.
12. Sponsoring Organization Name and Address As above			13. Type of Report & Period Covered 14.

15. Supplementary Notes

16. Abstracts

The report contains information on aeronautics; astronomy and astrophysics; atmospheric sciences; chemistry; earth sciences and oceanography; electronics and electrical engineering; energy conversion; materials; mathematical sciences; cybernetics, computers; mechanical, industrial, civil, and marine engineering; methods and equipment; missile technology; navigation, communications, detection, and countermeasures, nuclear science and technology; ordnance; physics; propulsion and fuels; space technology; and scientists and scientific organization in the physical sciences.

17. Key Words and Document Analysis. 17a. Descriptors

USSR
Aeronautics
Astronomy
Astrophysics
Atmospheric Sciences
Chemistry
Computers
Cybernetics
Earth Sciences
Oceanography
Electronics
Electrical Engineering
Energy Conversion
Materials
Mathematics
Mechanical Engineering
Civil Engineering
Industrial Engineering
Marine Engineering
Methods
Equipment
Missile Technology
Navigation and Communications
Detection and Countermeasures
Nuclear Science and Technology
Ordnance
Physics
Propulsion and Fuels
Space Technology

17b. Identifiers/Open-Ended Terms

17c. COSATI Field/Group 01,03,04,07,08,09,10,11,12,13,14,16,17,18,19,20,21,22

18. Availability Statement	19. Security Class (This Report)	21. No. of Pages
For Official Use Only. Limited Number of Copies Available From JPRS	UNCLASSIFIED	104
	20. Security Class (This Page) UNCLASSIFIED	22. Price

THIS FORM MAY BE REPRODUCED

USCOMM-DC 14952-P72

JPRS L/8338

15 March 1979

TRANSLATIONS ON USSR SCIENCE AND TECHNOLOGY
PHYSICAL SCIENCES AND TECHNOLOGY

(FOUO 15/79)

CONTENTS

CONTENTS (Continued) Page

ELECTRONICS AND ELECTRICAL ENGINEERING

MATCHED SURFACE ACOUSTIC WAVE FILTER FOR LOW TRANSMISSION RATES

Moscow ELEKTROSVYAZ' in Russian No 11, 1978 pp 58-61

[Article by A. Ye. Znamenskiy and Ye. S. Murator]

[Text] An optimal receiver for relative phase transmissions contains a filter matched to baseband or radio-frequency pulses.

Filters matched to baseband pulses for low transmission rates R= 5~25 kbaud are made using active RC networks (hybrid construction) while those corresponding to high rates R> 1Mbaud are made using miniature lumped parameter multitapped delay lines.

In many cases equipment size is smaller and receiver circuitry is simpler, while its specifications are better when rf pulse-matched filters are used instead of baseband matched filters.

Surface acoustic wave (SAW) device technology is widely used in construction of rf pulse matched filters [1, 2, 3]. The advantages of SAW technology is fully evident at information transmission rates exceeding R=20~30 kbaud. The lower limit for these rates is defined by two factors: 1) permissible temperature deviation of the center frequency of the most stable (with respect to temperature) piezo-electric element (ST-cut of quartz at $-50 \leq t \leq +50°C$), and also 2) the actual dimensions of the working matched filter as will be shown.

SAW devices are highly stable in a wide temperature range, a fact which is very important at low information transmission rates, their manufacturing technology is highly developed, they are very reliable and small in size as compared with the dimensions of series 153, 155, and 157 microcircuits.

The SAW filter structure is shown in Fig 1 where 1) is an acoustic guide; 2) is an interdigital transducer (IDT); 3) is a wideband IDT; 4) is an absorbing layer. As we know the filter's amplitude-frequency charactertistic $H(\omega)$ and its pulse response h(t) are related by an inverse Fourier transform:

$$h(t)=\frac{1}{2\pi}\int_{-\infty}^{\infty}H(\omega)e^{j\omega t}\,d\omega. \qquad (1)$$

Moreover, there exists a singular relationship between the pulse response h(t) and the shape of the envelope of the ID electrodes. Electrodes are positioned at $T = 1/2f_o$ intervals along the acoustic guide, and the electrode length is proportional to h(t) at the corresponding reference point T_n (see Fig 1).

In general, during calculations involving h(t) it is also necessary to include the amplitude-frequency characteristic of a second IDT

$$H(\omega)=H_1(\omega)H_2(\omega). \qquad (2)$$

As a rule, in practice the second IDT has a much wider bandwidth so that the resultant amplitude-frequency characteristic is mainly defined by a single narrow-band transducer, i.e. $H(\omega) \approx H_1(\omega)$.

Basic requirements for matched filter parameters:

Center frequency of the passband, Hz	$f_o \pm 0.03R$
Form of amplitude-frequency characteristic	Sin x/x x=(f-fo)/fo
Frequency band between the zeros of the main lobe of Sin x/x, Hz	$2(R \pm 0.03R)$
Deviation of phase-frequency characteristic from liner response, degrees	$\pm$ 5
Insertion loss, db	$\leq$ 30
Relative level of crosstalk components, db	-20

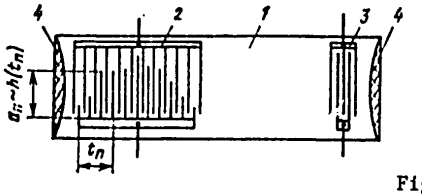

Fig 1

From this assumption it follows that the desired pulse response h(t) is fully defined by the shape of the envelope of the distributed transducer electrodes.

The greatest difficulties are encountered during manufacture of SAW filters at the lower end of realizable transmission rates (R = 20 ~ 30 kbaud). The amplitude-frequency response of a filter matched to a rectangular pulse is $H(\omega) = \text{Sin } x/x$ where the pulse width is defined as:

$$\tau = 1/R. \qquad (3)$$

Since a reduction of R leads to an increase in the transducer length l; $l = \tau v$ where v is the velocity of propagation of the surface wave in the acoustic guide. Thus, for R = 25 kbaud where v = 3,158 mm/μSec in an ST-cut quartz $l \approx 126$ mm. If we consider that the acoustic guide must be even longer by about 20 ~ 30 mm, then it is evident that such a filter is not an optimum one.

A second deficiency of the filter shown in Fig 1 is the difficulty of tuning a center frequency with high accuracy. It is shown that the velocity deviation in quartz acoustic guides is on the order of 10^{-4}. From the above it is clear that even if deviations involved during filter manufacture are excluded, it is very difficult to obtain the required accuracy for f_o at low transmission rates. Although methods used for tuning are known [4] these were carried out on small-size acoustic guides (i.e. for those used in high transmission rates). The method of applying a uniform-thickness metalized layer over the entire acoustic structure and the aging of this layer remains questionable.

A method is described below for making matched filters for low transmission rates which permits a reduction in the length of the acoustic guide by a factor of 2 and which allows for tuning the filter's center frequency while using relatively simple manufacturing methods.

The complex transfer function of IDT using equidistant electrode spacing and a constant aperture may be expressed as [5]

$$\overline{H}(\omega) = H_o \frac{\sin \frac{\omega\tau}{2}}{\frac{\omega\tau}{2}} e^{j\omega t + \frac{\omega\tau}{2}} \qquad .(4)$$

where H_o is a constant multiplier; t is the time; and $\omega = 2\pi(f - f_o)$.

Dropping the $e^{i\omega t}$ multiplier, which corresponds to a linear phase characteristic, for the sake of simplicity, expression (4) may be presented as:

$$\overline{H}(\omega)=H_0 \quad \frac{\sin\frac{\omega t}{4}}{\frac{\omega t}{4}} e^{\frac{i\omega t}{4}} \qquad 1+e^{\frac{i\omega t}{2}} \quad .$$

The first term corresponds to a transfer function of a matched filter for a transmission rate equal to R = 2/t; while the second term may be considered a transfer function of a transducer consisting of 2 IDTs shifted with respect to one another by $\tau/2$. The general form of these IDTs is similar to the characteristic of comb filters.

Figure 2 shows the structure of a matched filter for R = $1/\tau$ rate, synthesized by cascading a matched filter (in the upper part of the Fig) for R = $2/\tau$ rate and a comb filter (in the lower part of the Fig) where 1) is the acoustic guide; 2) is the shaping IDT of the matched filter for rate 2R; 3) is a wideband IDT; 4) is an absorbing layer; 5) is a shaping IDT of a comb filter; 6) is a mettalic layer.

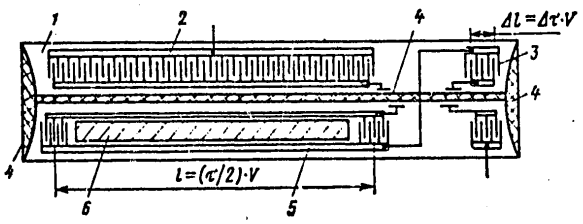

Fig 2

Both circuit sections are laid out on a single acoustic guide and are connected electrically. An absorbing layer is deposited between circuits to eliminate acoustic cross-talk between channels.

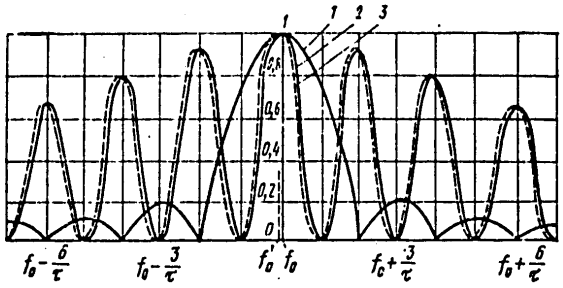

Fig 3

In comparison with a single section matched filter with transducer length equal to $\tau = 1/R$, a two-section construction permits a reduction in length by a factor of almost 2 (the higher R, the closer to 2).

In the above-described method of synthesis of a matched filter for low transmission rates permits, to a certain extent, varying the filter's center frequency. This is accomplished by changing the distance $\tau/2$ between transducer sections in the comb portion of the filter at the expense of increasing or decreasing the propagation velocity of the SAW in this region. It is known that the presence of a metalized layer in the propagation path of a SAW changes its velocity [6]. Thus, if a section of a continuously metalized layer between transducer sections is removed or deposited (see Fig 2) it is possible to vary the center frequency of the main amplitude-frequency response peak of the comb filter inside the wider amplitude-frequency response of the matched filter with $R = 2/\tau$. Corresponding amplitude-frequency characteristics are shown in Fig 3 where 1) is the amplitude-frequency characteristic of the matched filter for rate equal to 2R; 2) is the amplitude-frequency characteristic of the comb filter before returning; 3) is the amplitude-frequency characteristic of the comb filter after retuning.

In fact, at the center frequency f_o phasing condition $2\pi\left(\frac{\tau}{2} / \frac{1}{f_o}\right) = 2n$ is achieved (n is a whole number). Thus, $f_o = 2n/\tau$. At the same time $\tau/2 = L/V$ where L is the distance between centers of the comb filter sections; V is the propagation velocity of the SAW.

Deposition (removal) of the layer causes a corresponding reduction (increase) of the velocity in the region between sections V_{equiv}. Then

$$f_0 = \frac{n(V \pm \Delta V_{экв})}{L}.$$

This method of frequency tuning is not optimal because of a certain assymetry of side lobes. But, since the principal portion of the signal energy is concentrated in the center lobe it is more important to tune to the center frequency even at the expense of a certain deviation in the level of sidelobes from the design values in the range of $\pm$ 3db, a fact which was confirmed experimentally.

It is noted that the formulas used for synthesis of matched filters cited here do not include the finite length of small electrodes, i.e. wideband transducers in the two-section structure. This is deemed permissible where the relationship $\Delta\tau \ll \tau/2$ holds.

Second-order effects (spreading and scattering losses, losses due to dispersion of the acoustic wave by the IDT grating in lieu of electrical and mechanical surface loading), the influence of matching networks on the input and output [7] cause distortions in the amplitude-frequency characteristic

response and an increase in crosswalk levels. These effects increase with decreasing R. In order to reduce these effects it is necessary to introduce corrections in the transducer aperture and to utilize a construction with split electrodes, and also to consider the amplitude-frequency characteristics of the electrical circuits on the filter's input and output.

Experimental results.

The constructed matched filter was designed for two information transmission rates R_1 = 256 kbaud; R_2 = 64 kbaud and f_o = 12 MHz. Calculations have indicated that the dimensions of the filter are optimal if one of its parts is made using a two-section structure (for R_2 = 64 kbaud rate) and the second - using a single section (for R_1 = 256 kbaud rate) with subsequent positioning of both parts on a single acoustic guide (Fig 4).

The filter was constructed using a thermally stable SR-cut quartz plate measuring 45X20X2.5 mm. The IDT structure was formed using metal photoetching techniques on chemically deposited silver 0.1 μ thick. Aperture of all IDTs was 0.3 mm. The number of electrodes making up the R_1 IDT section was 47, which agrees with the given information transmission rate, and in the case of R_2 - 94, which corresponds to the doubling of the transmission rate.

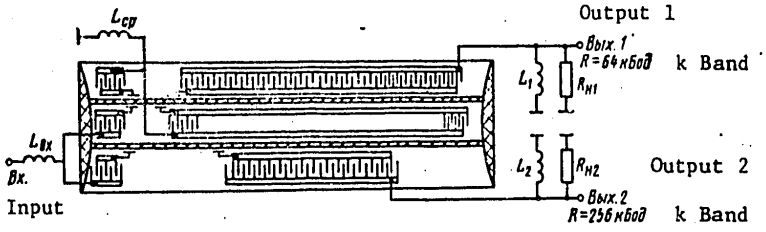

The absorbing layer was deposited at the ends of the acoustic guide at interchannel spacing using the FL - 03 coating in order to reduce crosstalk.

In order to reduce the insertion losses of the filter, its static transducer capacity was compensated by inductances. The input resistance of emitter followers were used as high impedance loads. The losses in the band of interest were 18 ± 2db. Deviation of side-lobe levels of the function Sin x/x from the theoretical values in the ± 3R range of tuning did not exceed 1db. Other parameters emt the given requirements.

The two-section matched filter was designed for R = 25.6 kbaud f_o = 12MHz. An SR-cut quartz plate measuring 80X20X5 mm was used for the acoustic guide. Filter structure was two-sectional. The above-described construction tech-

nique was utilized. The aperture for all IDTs was 4 mm. There were 235 electrode pairs in the shaping IDT which corresponds to a doubling of information transmission rate. Filter coupling into the RF strip and the static transducer capacitance compensation method did not differ from those in Fig 4 for R = 64 kbaud. Losses at the center frequency of the passband of interest were 14 ± 1db. Deviation of side lobes of the function Sin x/x in the ± 3R range of tuning did not exceed 2 db. Other parameters met the given requirements.

Thus, experimental characteristics of small-size filters with simple center frequency tuning agree fairly well with results of calculations according to given formulas.

The authors consider it their pleasant duty to express appreciation to A. F. Beletski for his careful review of the manuscript and his observations which have helped improve the quality of the article.

BIBLIOGRAPHY

1. Znamenskii A. E., "Fil'try poverkhnostnykh akusticheskikh voln" ["Surface acoustic wave filters"] ELEKTOSVYAZ', 1977, No 12.

2. Hays R., Hartmann C. "Surface acoustic wave devices for communications" Proceeding of the IEEE, 1976, Vol 64, No 5.

3. Dodonov A. B. et al. "Kompleksnaya mikrominiaturizatsiya priyemousilitel'nykh traktov na osnove integral'nykh sredstv chastotnoy selektsii" ["Complex microminiaturization of receiver sections using frequency selective integrated devices"] ELEKTRONNAYA TEKHNIKA Series 11, 1976, 3rd edition (7).

4. Hayde W., "Precision narrowband surface wave bandpass filters" 1974 Ultrasonics Symposium, Proceedings of the IEEE, Boston.

5. A. De Vries et al. "Characteristics of surface wave integratable filters" IEEE Transactions, 1971 Vol BTR-17, No 1.

6. Karinskiy S. S. "Ustroystvo obrabotki signalov na ul'trazvukovykh poverkhnostnykh volnakh" ["Signal processing devices using ultrasonic surface waves"] M., SOV. RADIO 1975.

7. Bondarenko, V. S. et al "Osobennosti raboty uzkopolosnogo fil'tra poverkhnostnykh akysticheskikh voln v razlichnykh rezhimakh nagruzki" ["Performance peculiarities of narrowband surface acoustic wave filter at different loads"] VOPROSY RADIOELEKTRONIKI: SER OBSHCHETEKHNICHESKAYA, 1976, Ed 7.

Submitted Oct 6, 1977

6981
CSO: 1870

ELECTRONICS AND ELECTRICAL ENGINEERING

NONCOHERENT RADAR SYSTEMS

Moscow RADIOTEKHNIKA i ELEKTRONIKA in Russian No 11, Nov 78 pp 2306-2313

[Article by V. V. Karavayev and V. V. Sazonov: "On the Theory of Non-Coherent Detection"]

[Text] The use of phased transmitting antenna arrays has several shortcomings in scanning space. Some of these shortcomings are as follows: energy dissipation in shaping a coherent probe signal in each element of the active array, and concentration of the beam to intensify emissivity due to increased antenna dimensions. In order to surmount these shortcomings, in [1] it was proposed to drop the phasing of individual elements of the transmitting array, avoid emitting signals with different (perhaps, random) modulation relationships; but coherent processing of the received signal was do be done with the aid of a set of reference signals generated for each angular bearing by a special device based on known or measured time relationships of amplitudes and phases of excitation of each emitter. Modulation of probe signals is needed to suppress gaps in transmitter directionality in non-cophase power conditions. A deficiency in this arrangement is the complex nature of producing a set of adjustable matching filters. Consequently, it is worth considering the characteristics of a system which does not employ time-matched filtration of an incoming noise signal (replacing it with band filtration). We shall demonstrate that with an optimum selection of system parameters, power losses due to noncoherent processing are not great.

If the transmitting antenna array is not phased, scintillation of the target can be suppressed by separation of the transmitters. Two versions of a transmitting system design will be examined below, differing in the manner of separation of the probe signal. In the first version, several spatially-separated transmitters are employed which simultaneously irradiate the target at different angles. In the second version, the transmitters are superposed, but a multiple frequency probe signal is utilized. Formulation of this problem here differs from that usually found in the literature (cf., for example, [2]) in that the incoming signal here has double modulation with different inherent times, occurring as a result of the random field of the transmitter and coefficient of reflection of the target.

1. THREE-DIMENSIONALLY SEPARATED SYSTEM

Let us consider that the processing channel contains a filter whose bandwidth matches the spectrum of the emitted signal; connected to its output are a square-law detector and a signal-length memory. The output effect of this processing is

$$z = \int_0^T |s(t)+\eta(t)|^2\,dt, \tag{1}$$

where s(t) and (t) are independent signal and noise components of the filtered out input process and T is processing time. In conformity with the above, the signal component may be represented in the form

$$s(t) = \sum_{j=1}^{n} \sqrt{\sigma_j}\, e^{i\theta_j} s_j(t), \tag{2}$$

where $s_j(t)$ is a random signal emitted by the j-th transmitter; n is their number; σ_j is the effective cross section of the target towards the receiver when it is irradiated by the j-th transmitter; and θ_j is the phase shift occurring with reflection from the target.

With fixed coefficients $A_j = \sqrt{\sigma_j} e^{i\theta_j}$ in (2) and large n, signal s(t) may be considered gaussian. In this case the distributive function of the quantity z is well described by the principle χ^2:

$$p(z/\{A_j\}) = \frac{z^{m-1} e^{-z/2\sigma^2}}{\sigma^{2m} 2^m \Gamma(m)}, \tag{3}$$

where 2m is the number of degrees of freedom and σ^2 is dispersion per degree of freedom. These parameters are expressed through the effective band of the signal Δf and signal dispersion σ_s^2 and noise σ_η^2 in the following manner: $m = \Delta f T$, $\sigma^2 = \sigma_s^2 + \sigma_\eta^2 = (\overline{|s|^2} + \overline{|\eta|^2})/2\Delta f$.

It is usually considered that the coefficients of reflection of target A_j are normal. For the same reason, if all A_j are independent and have identical dispersions, then the random quantity σ_s^2 is distributed according to the principle χ^2 with N = 2n degrees of freedom and dispersion ρ^2 per degree.

The characteristic function z is obtained by averaging the arbitrary characteristic function $c(u/\sigma_m^2) = (1 - iu2(\sigma_s^2 + \sigma_\eta^2)^{-m}$ in terms of the distribution σ_s^2. Let us find

$$c(u) = \frac{\left(\frac{\sigma_\eta^2}{2\rho^2} + \frac{i}{4\rho^2 u}\right)^{(n-m-1)/2} \times \exp\left(\frac{\sigma_\eta^2}{4\rho^2} + \frac{i}{8\rho^2 u}\right) W_{(1-n-m)/2,(n-m)/2}\left(\frac{\sigma_\eta^2}{2\rho^2} + \frac{i}{4\rho^2 u}\right)}{(-i4\rho^2 u)^m}, \tag{4}$$

where $W_{i,k}(x)$ is the Whittaker function. To derive the distributive law it is necessary to transform (4) according to Fourier. In the general case this can not be done. But in the detection problem the case where the signal significantly exceeds noise is most substantial; here noise affects ıly the choice of threshold. And in examining the statistics of the signal, noise may be ignored. Then

$$p(z)=\frac{z^{[(n+m)/2-1]}K_{n-m}\left(\sqrt{\frac{z}{\rho^2}}\right)}{\Gamma(n)\Gamma(m)2^{n+m-1}\rho^{n+m}}, \tag{5}$$

where $K_{-\nu}(x)$ is a Macdonald function.

In the absence of a signal, z is distributed according to the χ^2 principle. Therefore, probability of a false alarm is equal to

$$F=\int_{c}^{\infty}\frac{z^{m-1}e^{-z/2\sigma_\eta^2}}{2^m\Gamma(m)\sigma_\eta^{2m}}dz=\int_{c^*}^{\infty}\frac{x^{m-1}e^{-x/2}}{2^m\Gamma(m)}dx, \tag{6}$$

where $c^* = c/\sigma_\eta^2$, c is detection threshold. Probability of detection is equal to

$$D=\int_{c_*}^{\infty}\frac{x^{m+n-1}K_{n-m}(x)dx}{\Gamma(m)\Gamma(n)2^{n+m-2}}, \tag{7}$$

where $c_* = \sqrt{c'\sigma_\eta^2/\rho^2}$. This integral, for integral and half-integral values of m is reduced to tabular definitions. For integral m

$$D=\frac{c_*^{m+n-1}}{\Gamma(n)2^{m+n-2}}\sum_{l=0}^{m-1}\frac{2^l K_{n-m+l+1}(c_*)}{c_*^l\Gamma(m-l)}, \tag{8}$$

while for half-integral m

$$\begin{aligned}D=&\frac{(2m-2)!!}{\Gamma(m)\Gamma(n)2^{m+n-2}}\times\\ &\times\left[c_*^{m+n-1}\sum_{l=n}^{2m-2}\frac{K_{n-m+l+1}(c_*)}{c_*^l(2m-2(l+1))!!}+\right.\\ &+2^{(2n-3)/2}\sqrt{\pi}\,\Gamma\left(\frac{2n-1}{2}\right)(1-K_{n-\frac{1}{2}}(c_*)L_{n-\frac{1}{2}}(c_*)-\\ &\left.-L_{n-\frac{1}{2}}(c_*)K_{n-\frac{1}{2}}(c_*))\right].\end{aligned} \tag{9}$$

Here $L_{\nu}(x)$ is a Struve function.

The relationship $P(c_*) = 1 - D(c_*)$ as a function of c_* is given in Figures 1 and 2 for n = 3 and 5 and m = 1, 2, 3, 5, 10.

It is worth comparing the derived detection characteristics with those of the system in which emission and reception of the signal occurs coherently and where, as in the system in question, separation of signal through independent channels is utilized. In this instance, with quadratic composition, the distribution of the output effect is described by χ^2 with 2n degrees of freedom, while the detection characteristics are given by the formulas in [2]

(10)
$$F = \int_{c^*(n)}^{\infty} \frac{x^{n-1}e^{-x/2}}{2^n\Gamma(n)}dx,$$
$$D = \int_{c^*(n)/(1+\mu)}^{\infty} \frac{x^{n-1}e^{-x/2}}{2^n\Gamma(n)}dx,$$

where μ is the sum signal-to-noise ratio, defined as $\mu = n\mu_j$; μ_j is the average signal-to-noise ratio in the j-th channel.

A comparison of the detection characteristics of noncoherent and coherent systems shall be done for identical energies of the signal arriving at the input. In this case, the ordinates of the curves in Figures 1 and 2 are defined at points $c_* = \sqrt{2mnc^*(n)/\mu}$, and $c^*(n)$ is derived according to formula (10) for given F and n. Examples of the relationship of the threshold signal-to-noise ratio versus m are cited in Figures 3 and 4 for n = 3 and n = 5, respectively. It can be seen that for each value of n there exists an optimum m at which the threshold level of the signal is minimal. Here, in the form of horizontal lines, are also depicted the threshold characteristics of a coherent system. Minimal losses are defined by the distance from these lines to the extreme points of the corresponding curves. This losses are obviously not great. For D = 0.5 they are (-0.6 to + 0.6 dB) and for D = 0.99 they rise to 2.4 to 2.6 dB.

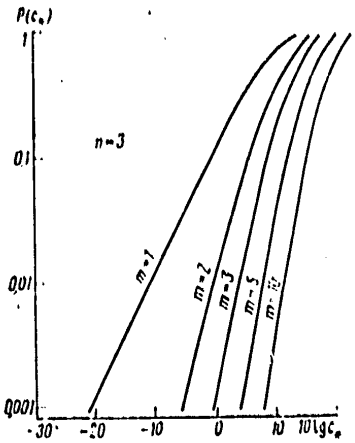

Figure 1

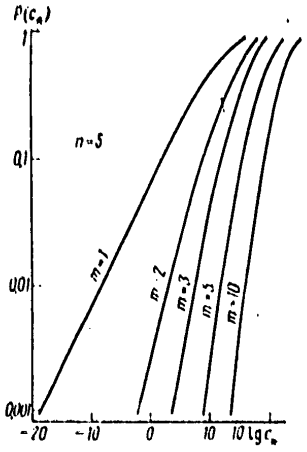

Figure 2

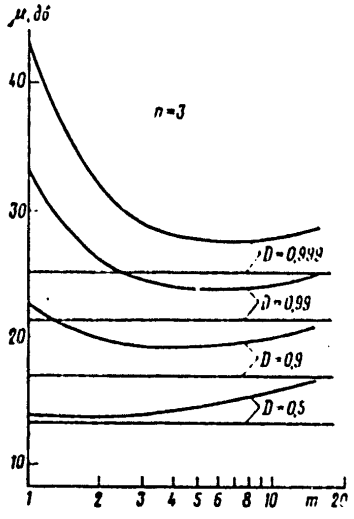

Figure 3

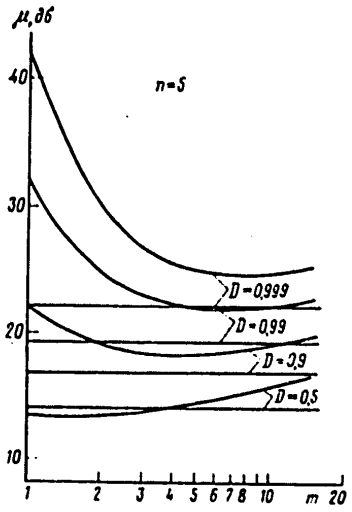

Figure 4

2. SYSTEM WITH FREQUENCY SEPARATION

To suppress fluctuations of a Rayleigh target, this system utilizes frequency retuning of the signal from impulse to impulse. Processing consists of band filtration of each frequency channel, square-law memory of signal duration and memory of frequency channels.

Consequently, the output effect of this system appears as

$$z = \sum_{j=1}^{n} z_j = \sum_{j=1}^{n} \int_0^T |A_j s_j(t) + \eta_j(t)|^2 \, dt, \tag{1}$$

where $s_j(t)$ and $\eta_j(t)$ are independent signal and noise components in the band Δf of the j-th frequency channel and A_j is the random coefficient of reflection of the target at the j-th frequency. We shall assume that frequency separation is chosen so A_j are independent.

At fixed values of A_j the quantities z_j, as before, may be considered as distributed according to χ^2 with $2m = 2\Delta fT$ degrees of freedom. Consequently, the arbitrary (for given A_j) characteristic function of quantity z_j is given by the expression

$$c_{z_j}(u/\{A_j\}) = [1 - 2iu(|A_j|^2\sigma_1^2 + \sigma_0^2)]^{-m}, \tag{12}$$

where σ_1^2 and σ_0^2 are dispersions per degree of freedom of signal $s_j(t)$ and noise $\eta_j(t)$, respectively. The absolute characteristic function is obtained by averaging (12) in terms of the distribution of the random quantity $|A_j|^2$ (scattering cross section) which we, as before, consider to be exponential with average unit power. Employing [3], we find

$$c_{z_j}(u) = \int_0^\infty \frac{e^{-y}\,dy}{[1 - 2iu(\sigma_1^2 y + \sigma_0^2)]^m} = \frac{e^{[2iu\sigma_0^2 - 1)/2iu\sigma_1^2]}\,\Gamma\left(1 - m, \dfrac{2iu\sigma_0^2 - 1}{2iu\sigma_1^2}\right)}{(-2iu\sigma_1^2)^m} \tag{13}$$

where $\Gamma(\nu, x)$ is an incomplete gamma function.

(14) $$D=\int_c^\infty p(z)\,dz=1-\frac{1}{2\pi}\int_0^c\int_{-\infty}^{\infty}c_1(u)\,e^{-iuz}\,du\,dz=$$

$$=1-\frac{1}{2\pi}\int_{-\infty}^{\infty}\frac{\exp\left[n\dfrac{2iu\sigma_0^2-1}{2iu\sigma_1^2}-\dfrac{iuc}{2}\right]}{(-2iu\sigma_1^2)^{mn}}\times$$

$$\times\Gamma^n\left(1-m,\ \frac{2iu\sigma_0^2-1}{2iu\sigma_1^2}\right)\frac{\sin\dfrac{uc}{2}}{\dfrac{u}{2}}\,du,$$

where c is the threshold defined by the required value of false alarm. This integral can be computed only for n = 1. Thus we calculated the characteristics of detection by constructing an integral law of distribution of the quantity z using the method of mathematical simulation. Being concerned with a region of rather high probability of detection and small false alarms at that, we will, as earlier, consider noise only in calculating threshold. Notably, the integral law of distribution was calculated of the quantity

(15) $$\zeta=\sum_{j=1}^{n}|a_j|^2\sum_{k=1}^{m}|b_{jk}|^2,$$

where a_j and b_{jk} are independents for different j and k and one from another are random quantities with unit dispersions of the quadrature terms.

Integral laws $P(\zeta)$ for various m and n = 3 and n = 5 are shown in Figures 5 and 6 as a function of $10\log\zeta$. Using these graphs it is easy to construct characteristics of detection for any probability of false alarm which, as before, is given by the integral law χ^2 (6), but now with 2mn degrees of freedom:

(16) $$F=\int_{c}^{\infty}\frac{z^{mn-1}e^{-z/2\sigma_0^2}\,dz}{2^{mn}\Gamma(mn)\sigma_0^{2mn}}=$$

$$=\int_{c^*}^{\infty}\frac{x^{mn-1}e^{-x/2}}{2^{mn}\Gamma(mn)}\,dx,\quad c^*=\frac{c}{\sigma_0^2}.$$

Probability of detection is then derived according to

(17) $$D=1-P_\zeta\left(\frac{c^*2mn}{\mu}\right)$$

where μ, as before, is the sum signal-to-noise ratio.

When the latter formula and Figures 5 and 6 are utilized, relationships of threshold signal-to-noise ratio for various probabilities of detection are obtained as a function of the number m of time cells in each frequency channel. They are shown in Figures 7 and 8 for n =3 and n = 5 with a probability of false alarm $F = 10^{-6}$. Characteristics of detection of a coherent system (horizontal lines) with the appropriate number of independent separation channels n are given here for comparison.

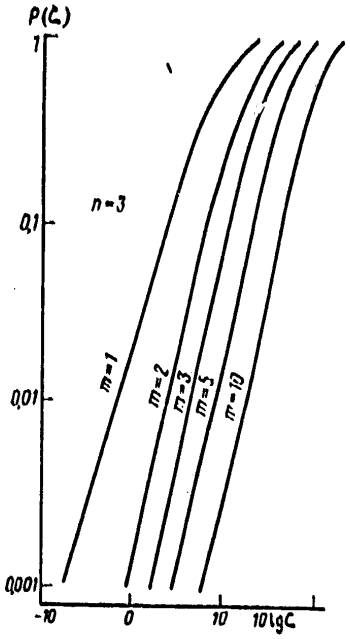

Figure 5

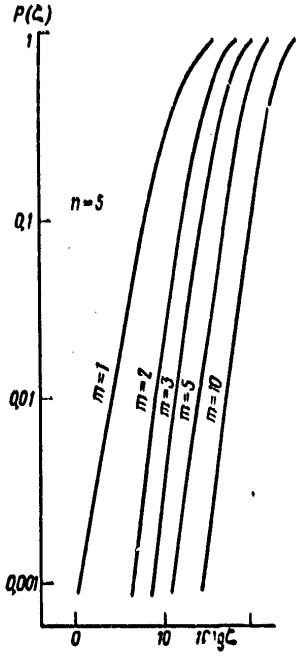

Figure 6

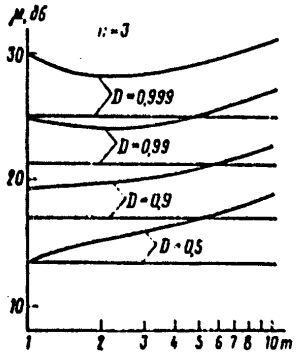

Figure 7

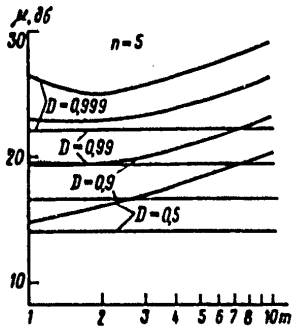

Figure 8

The figures presented show that just as in the case of three-dimensional separation, with increase m (for given n) losses in μ for D $\gtrsim$ 0.5 at first decrease and then grow. But this effect is manifested more sharply. It is associated with the fact that the quantity of noncoherently stored discrete units with frequency separation is equal to mn, whereas in three-dimensional separation it is equal to m. Consequently, in the first case, due to noncoherent storage, losses being to show at much lower values of m. Accordingly, optimum values of m lie between one to two (versus 5 to 10 for three-dimensional separation), and losses are slightly higher (by 0.5 to 1 dB).

CONCLUSION

The characteristics of detection of a Rayleigh target by radar location are examined: there is no phasing of components of the transmitting system. For the case of great three-dimensional separation of transmitters, analytical expressions are obtained which describe the characteristics of detection. For the case of frequency separation the appropriate formulas are derived in quadratures, and calculation of characteristics of detection was done by the method of mathematical simulation.

It was found that with optimum selection of the band of a random probe signal and number of branches of separation, abandonment of the use of phasing does not lead to substantial losses in the signal-to-noise ratio. According to the probability of detection, they range from 0.5 to 3 dB. A system with three-dimensional separation has minimal losses.

The authors express their gratitude to I. G. Korobkova, who performed the calculations on computer.

REFERENCES

1. H. H. Woerrlein, Pat. USA No. 3, 680.100, 25 Jul 72.
2. P. A. Bakut, I. A. Bol'shakov, B. M. Gerasimov et al. Problems of statistical theory of radiolocation [Voprosy statisticheskoy teorii radiolokatsii], 1, Izd. Sovetskoye radio, 1963.
3. I. S. Gradshteyn, I. M. Ryzhik, Tables of integrals, sums, series and derivations [Tablitsy integralov, summ, ryadov i proizvedeniye], 4th ed., GIFML, 1962.

8617
CSO: 1870

ELECTRONICS AND ELECTRICAL ENGINEERING

RANGE AND BEARING ACCURACY USING ANTENNA ARRAYS

Moscow RADIOTEKHNIKA i ELEKTRONIKA in Russian No 11, Nov 78 pp 2314-2320

[Article by I. Ya. Kremer and G. S. Nakhmanson: "On the Potential Accuracy of Estimating Range and Angular Coordinate of a Target with Signal Reception by an Antenna Array in the General Case"]

[Text] INTRODUCTION

The primary current assumptions of the theory of time-space processing of signals [4, 2] are valid for arbitrary time-space signals. But specific results in the literature have mainly been obtained as they apply to the special case where the wave fronts of signals can be considered flat, i.e., the signal sources are in the remote zone of the receiving antenna. If the signal source is situated in the Fresnel zone of the receiving antenna, an estimate of the parameters of time-space signals has substantial peculiarities associated with the curvature of the signal wave front. These distinctive aspects have been investigated in studies [1, 2, 6] as they apply to antennas with continuous linear apertures.

In this article the potential accuracy of estimates of range and angular position of a target are considered for reception of signals by an antenna array in the general case, which includes positioning of the target both in a remote zone and in a Fresnel zone. The rise in potential accuracy of range analysis owing to consideration of signal wave front curvature is analyzed as a function of the number of array elements. The ambiguity of range measurement is considered for reception in "widely spaced" arrays and conditions to eliminate this problem are discussed.

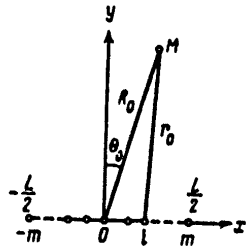

Figure 1

1. POTENTIAL ACCURACY OF ANALYSIS OF TARGET COORDINATES WITH SPACE & TIME PROCESSING OF SIGNALS IN AN ANTENNA ARRAY

Let us consider an equidistant linear array whose length is L and whose distance between elements is d having N = 2m + 1 elements (Figure 1).

Let us first consider the case of active location. A sounding signal is emitted from point 0

(1) $$s(t)=U(t)\cos[\omega_0 t+\Phi(t)].$$

A small target is situated at point M with coordinates (R_0, Θ_0). The vector the arriving signal may then be represented as

(2) $$\|x_i(t)\|=\|s_i(t, R_0, \Theta_0, \varphi_0)\|+\|n_i(t)\|,$$

where i = -m, ..., 0, ...; m is the number of the receiving array element.

In formula (2) $\|n_i(t)\|$ is a vector of gaussian interference with zero average values and correlation matrix $\|B_{ij}(t_1,t_2)\| = \|\langle n_i^T(t_1) \otimes n_j(t_2)\rangle\|$; T denotes the operation of transposition, and $\otimes$ is the direct Kronecker product of the vectors. Henceforth we shall consider that $B_{ij}(t_1,t_2) = (N_0/2) \times \delta(t_1 - t_2)\delta_{ij}$, i.e., interference in various elements of the array is not correlated and in all elements has an identical correlation function. Components of the signal vector are

(3) $$s_i(t, R_0, \Theta_0, \varphi_0)=a_0 U\left(t-\frac{R_0+r_{0i}}{c}\right)\cos\left[\omega_0\left(t-\frac{R_0+r_{0i}}{c}\right)+\right.$$
$$\left.+\Phi\left(t-\frac{R_0+r_{0i}}{c}\right)-\varphi_0\right]$$

where φ_0 is random initial phase, uniformly distributed in interval $[0, 2\pi]$; a_0 is signal amplitude; r_{0i} is distance from the target to the i-th receiving element of the antenna array, equal to*

(4) $$r_{0i}=r(id, R_0, \Theta_0)=\sqrt{R_0^2+(id)^2-2idR_0\sin\Theta}$$

* In formula (3), the relationship of signal amplitude of the i-th element as a function of distance r_{0i} is not considered, since it can be shown that this relationship has very little effect on the final results where $R_0 > L$.

When receiving a mixture of (2), the optimum receiver shapes an output signal proportional to the log of the functional of the likelihood ratio [3]:

(5) $$M(R,\Theta)=\ln I_0\left[\frac{2a_0}{N_0}Z(R,\Theta)\right],$$

where I_0 is a zero order Bessel function from an imaginary independent variable; $Z(R, \Theta)$ is the envelope of a random process at the output of the linear portion of the receiver, defined by the relationship

(6) $$Z(R,\theta)=\left|\sum_{i=-m}^{m}\int_0^T x_i(t)\dot{U}\left(t-\frac{R+r_i}{c}\right)\exp\left\{-j\omega_0\left(t-\frac{R+r_i}{c}\right)\right\}dt\right|;$$

r_i is defined by expression (4) for arbitrary values of R and Θ.

In measurement of signal parameters according to the method of maximum likelihood under conditions of reliable measurement (i.e., large signal-to-noise ratios at receiver output), estimates of R_m and Θ_m are unbiased with dispersions, whose expressions in the first approximation have the appearance [3,4]

(7) $$\sigma_R^2=[B_{RR}(1-\rho^2)]^{-1},\ \sigma_\Theta^2=[B_{\Theta\Theta}(1-\rho^2)]^{-1},\ \rho=B_{R\Theta}(B_{RR}B_{\Theta\Theta})^{-1/2},$$

where $$B_{\nu q}=\left[\frac{\partial^2 G(\vec{l}_1,\vec{l}_2)}{\partial l_{1\nu}\partial l_{2q}}\right]_{\vec{l}_1=\vec{l}_2=\vec{l}_0};\ \vec{l}=(R,\Theta),$$

(8) $$G(R_1,\Theta_1,R_2,\Theta_2)=\left|\sum_{i=-m}^{m}\frac{a_0^2}{N_0}\int_0^T\dot{U}\left(t-\frac{R_1+r_{1i}}{c}\right)\times\right.$$
$$\left.\times\dot{U}\left(t-\frac{R_2+r_{2i}}{c}\right)\exp\left\{j\omega_0\frac{R_2-R_1+r_{2i}-r_{1i}}{c}\right\}dt\right|,$$

and indexes ν and q acquire the values of R, Θ. Substitution of (8) in (7) considering (4) yields

(9) $$B_{\nu q}=Q_0\left(\frac{\omega_0}{c}\right)^2\left[\frac{\Pi_0^2}{\omega_0^2}\gamma_{\nu q}+\gamma_{\nu q}-\gamma_\nu\gamma_q\right],$$

where $\Pi_s^2=4\pi^2\int_{-\infty}^{\infty}f^2|s(f)|^2df\Big/\int_{-\infty}^{\infty}|s(f)|^2df$ -- is the square of the equivalent width of signal spectrum s(f); $Q_0=(2m+1)Q_1$ -- is the signal-to-noise ratio at the receiver output; $Q_1=(a_0^2/N_0)\int_0^T U^2(t)\,dt$ is the signal-to-noise ratio at the output of an individual receiving element. Functions γ_{vq} and γ_v, γ_q in (9) are defined as follows:

$$\gamma_{RR}=(2m+1)^{-1}\sum_{i=-m}^{m}c_{iR}^2,\quad \gamma_R=(2m+1)^{-1}\sum_{i=-m}^{m}c_{iR},$$

$$\gamma_{\Theta\Theta}=(2m+1)^{-1}\sum_{i=-m}^{m}c_{i\Theta}^2, \tag{10}$$

$$\gamma_\Theta=(2m+1)^{-1}\sum_{i=-m}^{m}c_{i\Theta},\quad \gamma_{R\Theta}=(2m+1)^{-1}\sum_{i=-m}^{m}c_{i\Theta}c_{iR},$$

where $$c_{iR}=\left[\frac{\partial(R+r_i)}{\partial R}\right]_{R_0,\Theta_0};\quad c_{i\Theta}=\left[\frac{\partial(R+r_i)}{\partial\Theta}\right]_{R_0,\Theta_0}.$$

In considering the range of distances for which $L/R \ll 1$ is valid, $r_i(R, \Theta)$ may be expanded in terms of steps id/R:

$$r_i(R,\Theta)=R-id\sin\Theta+\frac{(id)^2}{R}\frac{\cos^2\Theta}{2}+\frac{\sin\Theta\cos^2\Theta}{2}\frac{(id)^3}{R^2}- \tag{11}$$
$$-\frac{1-5\sin^2\Theta}{8}\cos^2\Theta_0\frac{(id)^4}{R^2}+\ldots.$$

Allowing for (9)-(11), computation of dispersions of estimates (7) yields

$$\sigma_R^2=\frac{c^2}{\omega_0^2Q_0}\left\{4\frac{\Pi_s^2}{\omega_0^2}\left[1-\frac{B_1\alpha^2}{2(\Pi_s^2/\omega_0^2+1)}\left(\cos^2\Theta_0+\frac{\Pi_s^2}{\omega_0^2}+\right.\right.\right. \tag{12}$$
$$\left.\left.\left.+\frac{\Pi_s^2}{\omega_0^2}\sin^2\Theta_0\right)+\alpha^4\frac{B_2}{16}\cos^2\Theta_0(7-31\sin^2\Theta_0)\right]+\right.$$
$$\left.+\frac{\alpha^4}{4}(B_2-B_1^2)\cos^4\Theta_0\right\}^{-1},$$

(13)
$$\sigma_\theta^2 = \frac{c^2}{\omega_0^2 Q_0 (L/2)^2 \cos^2\Theta_0}\left\{D_\theta - \alpha^2 B_1^2 \frac{\Pi_0^2}{\omega_0^2}\sin^2\Theta_0\right\}^{-1},$$
$$D_\theta = \frac{\Pi_0^2}{\omega_0^2}[B_1 + \alpha^2(3\sin^2\Theta_0 - \cos^2\Theta_0)B_2] + B_1 +$$
$$+\alpha^2[\sin^2\Theta_0(3B_2 - B_1^2) - B_2\cos^2\Theta_0],$$
$$B_1 = \frac{1}{3}\left(1+\frac{1}{m}\right), \quad B_2 = \frac{1}{15}\left(1+\frac{3}{m}\right)\left(3+\frac{3}{m}-\frac{1}{m^2}\right),$$

$\alpha = L/2R_0$ is the ratio of antenna aperture size to distance to the target m = L/2d. Error in formulas (12) and (13) have an order of magnitude, respectively, of $O(\alpha^6)$ and $O(\alpha^4)$.

In passive location of an emission source with known signal shape, taking the center of the antenna aperture as the readout origin, a signal in the i-th receiving element may be written out as follows:

(14)
$$s_i(t, R_0, \Theta_0, \varphi_0) = a_0 U\left(t - \frac{r_{0i} - R_0}{c}\right)\cos\left[\omega_0\left(t - \frac{r_{0i} - R_0}{c}\right) + \right.$$
$$\left. + \Phi\left(t - \frac{r_{0i} - R_0}{c}\right) - \varphi_0\right].$$

By making transformations similar to earlier ones, it is not difficult to see that expressions for estimate dispersions for range and angular position coincide with (7), if in (1)

(15)
$$c_{iR} = \left[\frac{\partial(r_i - R)}{\partial R}\right]_{R_0,\Theta_0}, \quad c_{i\Theta} = \left[\frac{\partial(r_i - R)}{\partial\Theta}\right]_{R_0,\Theta_0}.$$

Substitution of (15) in (10), (7) yields

(16)
$$\sigma_R^2 = \frac{4c^2}{\omega_0^2 Q_0 \alpha^2 \cos^2\Theta_0}\left\{\frac{\Pi_0^2}{\omega_0^2}B_2 + B_2 - B_1^2\right\}^{-1}.$$

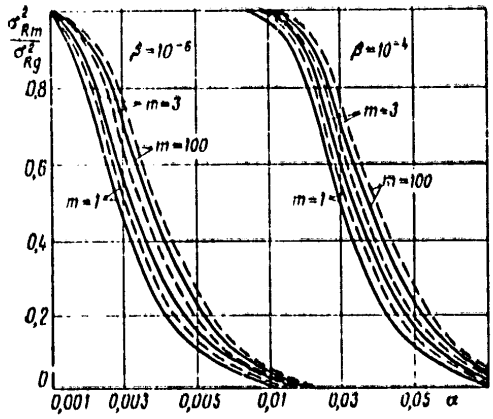

Figure 2

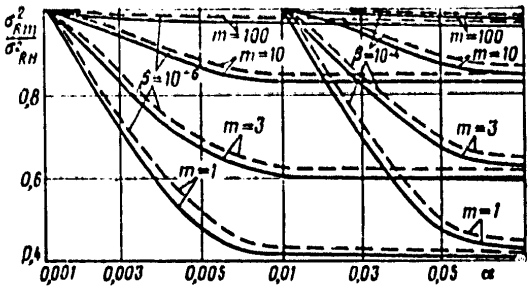

Figure 3

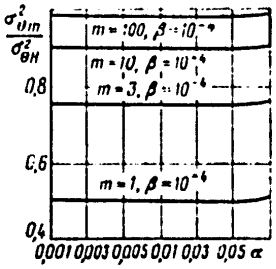

Figure 4

(17)
$$\sigma_{\theta}^2 = \frac{c^2}{\omega_0^2 Q_0 (L/2)^2 \cos^2\Theta} \times$$
$$\times \left\{ D_0 - \alpha^2 \frac{9\sin^2\Theta_0 \left(\frac{\Pi_3^2}{\omega_0^2} B_4 + B_2 - \frac{B_1^2}{3} \right)^2}{(\Pi_3^2/\omega_0^2 + 1) B_2 - B_1^2} \right\}^{-1}.$$

Where $m \to \infty$ (and condition $\lim_{\substack{m\to\infty \\ d\to 0}} 2md = L$), expressions (12), (13) and (16), (17) coincide with known ones obtained for a continuous aperture [1]. For transition to a remote zone ($R_0 \to \infty$, $\alpha \to 0$), expressions (12),(13) become

(18)
$$\sigma_{R_0}^2 = \frac{c^2}{4\Pi_3^2 Q_0}, \quad \sigma_{\theta_0}^2 = \frac{c^2}{\omega_0^2 Q_0 (L/2)^2 B_1 \cos^2\Theta_0} \left(\frac{\Pi_3^2}{\omega_0^2} + 1 \right)^{-1},$$

which coincides with expressions obtained in [2,4].

2. DISCUSSION OF RESULTS

For the case of active location, in Figure 2 is shown the ratio of estimate dispersions of target range for various values of the parameter of wide bandwidth $\beta = \Pi_3/\omega_0$ and for various values of the angle of signal arrival Θ_0, with optimum space and time processing of signals 2m+1 by receiving elements in an aperture L long (12), to the estimate dispersion of range for measurement of the latter according to a signal delay $\sigma_{R_0}^2$ (18) as a function of $\alpha = md/R_0 = L/2R_0$ (ratio if antenna aperture size to twice the distance to the target). The curves are constructed under the premise that the signal-to-noise ratio remains constant.

The solid curves correspond to the arrival angle $\Theta_0 = 0$, while the dotted curves are $\Theta = 24^\circ$. Figure 2 indicates that the gain in measurement accuracy of target range as α increases is proportional: this may be explained by the increased curvature of the front of the incident wave when the target approaches the receiving antenna. This gain increases with a decrease in Θ_0 and the parameter of wide bandwidth β as well. The ratio of estimate dispersion of target range with optimum space and time processing of signals by an antenna array containing 2m+1 receiving elements, to the estimate dispersion of range for signal processing in a continuous aperture of the same size for various values of parameters β and m as a function of α is shown in Figure 3. Analysis of curves in Figures 2 and 3 shows that with constant dimensions of an antenna system and identical values of signal-to-noise ratio Q_0, a reduction in the number of receiving elements leads to an increase in accuracy of range measurement.*

* In practice, the condition of sameness Q_0 may be ignored: the signal-to-noise ratio may be reduced with a reduction in the number of receiving elements (2m+1). In this case a reduction in accuracy caused by reduced Q_0 is, to some extent, equalized by raising accuracy as a result of a reduction in m shown in Figures 2 and 3.

When distances between antenna elements exceed the wavelength, ambiguity of range measurement by wave front curvature may occur. This ambiguity may be eliminated with combined measurement of range in terms of delay time and in terms of its wave front curvature. For this purpose, the signal spectrum width should be such that in measuring range by delay time of a signal, the magnitude of the resolution interval does not exceed the magnitude of interval of an unambiguous determination of range according to wave front curvature.

Let us determine the relationship of the required signal spectrum width as a function of antenna parameters and distance to target.

For a signal from the target located at a point having coordinates R_0, Θ_0, the phase difference between signals received by the m-th and (m-1)st elements will be

$$\Delta\varphi^{(1)} = \frac{2\pi}{\lambda_0}\left(d\sin\Theta_0 + \frac{2m-1}{2}\frac{d^2}{R_0}\cos^2\Theta_0\right), \tag{19}$$

where $\lambda_0 = c/f_0$ is wavelenght corresponding to carrier frequency.

If the target is located at point $R_0 + \delta R$, Θ_0, the phase difference has the magnitude

$$\Delta\varphi^{(2)} = \frac{2\pi}{\lambda_0}\left(d\sin\Theta_0 + \frac{2m-1}{2}\frac{d^2}{R_0+\delta R}\cos^2\Theta_0\right). \tag{20}$$

An unambiguous measurement of range occurs if the change in phase difference satisfies the condition $\delta\varphi = \Delta\varphi^{(1)} - \Delta\varphi^{(2)} < 2\pi$; the maximum interval of an unambiguous analysis of δR corresponds to the value $\delta\varphi = 2\pi$. From (19) and (20) it follows that $\delta\varphi = 2\pi$ when

$$\delta R = \frac{2R_0^2\lambda_0}{(2m-1)d^2\cos^2\Theta_0}. \tag{21}$$

On the other hand, when measuring range by delay time, the resolution interval is determined by the equation $\Delta R = c/2\Delta f$. Unambiguity of range

measurement according to wave front curvature will be eliminated by measurement of range by delay time, if $\Delta R < \delta R$. As follows from (21), this condition is met if

$$\beta = \frac{\Delta f}{f_0} \geqslant \frac{2m-1}{4R_0^2} d^2 \cos^2\theta_0 = \frac{2m-1}{16m^2}\left(\frac{L}{R_0}\right)^2 \cos^2\theta_0. \quad (22)$$

From equation (22) it is clear that for given antenna dimensions, the required value $\Delta f/f_0$ is inversely proportional to the number of receiving elements and the range.

Let us examine the effect of signal wave front curvature and antenna aperture discreteness on the potential accuracy of measurement of the target's angular coordinate. In Figure 4 is shown the ratio of $\sigma_{\theta m}^2/\sigma_{\theta H}^2$ of estimate dispersion of the angular coordinate as a function of α for reception of a signal by a linear antenna array consisting of 2m+1 elements, to estimate dispersion of the target's angular position in signal processing in a continuous aperture for various values of m. From Figure 4 it follows that, as in the case of estimating range, with given antenna system dimensions and identical values of signal-to-noise ratio, accuracy of measurement of the target's angular coordinate increase as the number of receiving elements decreases. Analysis of the possibility of measuring the angular coordinate shows that, in contrast to target range measurement, consideration of wave front curvature has almost no effect on the selection of a value for β, necessary for an unambiguous readout of angle; is defined by the relationship

$$\beta = \frac{\Delta f}{f_0} \geqslant \frac{1}{m}$$

which coincides with the results of [5]. In systems with a small number of receiving elements, when measuring bearing, in order to eliminate unambiguity it is necessary to have a substantial expansion of signal spectrum and the problem may be solved by using a multiple-frequency signal. In this instance, expression (22) remains true if the interval between the extreme scale frequencies is taken as Δf and the central frequency of this interval is taken as f_0.

CONCLUSION

Relationships obtained in this article allow us to determine the potential accuracy of range and angular coordinate estimates of a "point" target in the general case, including its position in both the remote and Fresnel zones

of the receiving antenna array. Furthermore, relationships suitable for the remote zone follow as a special case from relationships which are valid for the Fresnel zone.

Analysis of these relationships shows that in the Fresnel zone, the potential accuracy of range estimation rises (versus remote zone) owing to consideration of information included in the signal wave front curvature. This rise is even more substantial if the curvature of the wave front is greater; it also depends on the number of array elements. With a constant signal-to-noise ratio, potential accuracy is higher if the number of array elements is reduced. To some extent, this is compensation for a drop in accuracy which may arise due to the drop in signal-to-noise ratio when the number of array elements is reduced.

REFERENCES

1. I. Ya. Kremer, V. A. Pon'kin. Radiotekhnika i elektronika 1975, 20, 6, 1186.

2. Ya. D. Shirman. Resolution and compression of signals [Razresheniye i szhatiye signalov]. Izd. Sovetskoyet radio, 1974.

3. Ye. I. Kulikov. Estimating signal parameters in the presence of interference [Voprosy otsenok parametrov signalov pri nalichii pomekh], Izd. Sovetskoye radio, 1968.

4. S. Ye. Fal'kovich. Estimating signal parameters [Otsenka parametrov signala]. Izd. Sovetskoye radio, 1970.

5. Dausin, Naybar, Nilson. Zarubezhnaya radioelektronika, 1961, 4, 33.

6. I. Ya. Kremer, V. A. Pon'kin. Radiotekhnika i elektronika, 1977, 22, 1, 72.

8617
CSO: 1870

ELECTRONICS AND ELECTRICAL ENGINEERING

ELECTROMAGNETIC INTERACTIONS IN TRANSMISSION LINES

Moscow RADIOTEKHNIKA i ELEKTRONIKA in Russian No 11, Nov 78 pp 2363-2370

[Article by D. V. Sokolov, D. I. Trubetskov, Yu. P. Sharayevskiy and V. P. Shakhin: "Interaction of Electron Flux with High Frequency Fields of Coupled Transmission Lines. Type M Interaction"]

[Text] 1. FUNDAMENTAL EQUATIONS

As applied to type M beam-type devices, for simplicity we will take coupled transmission lines (CTL) to mean two identical electrodynamic structures, periodic along the x-axis, situated at some distance opposite one another, forming a combined wave-guide system (Fig. 1).

If we limit ourselves only to a consideration of three-dimensional harmonics of the high-frequency field in the CTL, then the corresponding components of intensity of the "cold" electrical field are expressed through the amplitudes of normal waves of the wave-guide system in question as follows [1]:

(1)
$$E_x = E_1(x)\frac{\operatorname{sh}\beta_1 y}{\operatorname{sh}\beta_1 a} + E_2(x)\frac{\operatorname{ch}\beta_2 y}{\operatorname{ch}\beta_2 a},$$
$$E_y = jE_1(x)\frac{\operatorname{ch}\beta_1 y}{\operatorname{sh}\beta_1 a} + jE_2(x)\frac{\operatorname{sh}\beta_2 y}{\operatorname{ch}\beta_2 a},$$

where

(2)
$$E_1(x) = E_{10}(x)e^{-j\beta_1 x},$$
$$E_2(x) = E_{20}(x)e^{-j\beta_2 x}.$$

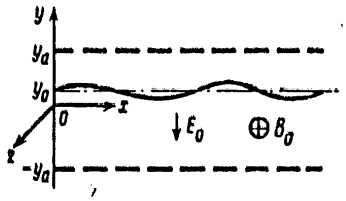

Figure 1. Schematic representation of electron flux interaction space moving in crossed fields with coupled transmission lines.

In expressions (1) and (2), the index 1 is related to an antisymmetrical normal wave occurring with antiphase excitation of both periodic structures; and index 2--to a symmetrical normal wave occurring in synphase excitation. Allowing for (1) and (2), the system of working equatios which describes interaction of electron flux in crossed fields with high-frequency fields of a CTL may be written as follows:

$$\frac{dX}{dq} = j\left[F_1\frac{\operatorname{ch} p_1 Y}{\operatorname{sh} p_1 Y_a} + F_2\frac{\operatorname{sh} p_2 Y}{\operatorname{ch} p_2 Y_a}\right]e^{-jX},$$

(3)
$$\frac{dY}{dq} = \left[F_1\frac{\operatorname{sh} p_1 Y}{\operatorname{sh} p_1 Y_a} + F_2\frac{\operatorname{ch} p_2 Y}{\operatorname{ch} p_2 Y_a}\right]e^{-jX},$$

$$\frac{dF_1}{dq} + jb_1F_1 = \frac{p_1\varkappa_1}{2\pi}\int_0^{2\pi}\frac{\operatorname{sh} p_1 Y}{\operatorname{sh} p_1 Y_a}e^{jX}\,dX_0,$$

(4)
$$\frac{dF_2}{dq} + jb_2F_2 = \frac{p_2\varkappa_2}{2\pi}\int_0^{2\pi}\frac{\operatorname{ch} p_2 Y}{\operatorname{ch} p_2 Y_a}e^{jX}\,dX_0.$$

In equations (3) and (4) the following designations are introduced:

$$X=\beta_e x-\omega t, \quad Y=\beta_e y, \quad F_{1,2}=\frac{E_{1,2}}{E_0 D_0}e^{-jb_{1,2}q},$$
$$q=\beta_e D_e x, \quad b_{1,2}=(\beta_{1,2}-\beta_e)/\beta_e D_e, \quad D_e^2=\beta_e I_e K_e/E_0,$$
$$K_e=(K_1+K_2)/2, \quad \varkappa_{1,2}=K_{1,2}/K_e, \quad p_{1,2}=\beta_{1,2}/\beta_e,$$

$K_{1,2}$ are coupling resistances of normal waves in planes $y = \pm a$, respectively. System of equations (3), (4) is written in adiabatic approximation, ignoring the effect of space charge on interaction processes.

2. ESTIMATED RELATIONSHIPS FOR WEAK SIGNAL CONDITIONS

Let us make some tentative estimates based on solution of system of equations (3)-(4) under weak signal conditions, using the method of successive approximations [2].

Assuming that $X = X_0 + \tilde{X}$, $Y = Y_0 + \tilde{Y}$ ($\tilde{X}$, $\tilde{Y} \ll 1$), F_1 and F_2 are constant in equation (3); by integrating (3)-(4) under the appropriate initial conditions ($q = 0$, $\tilde{X} = \tilde{Y} = 0$; $F_{1,2} = F_{1,20}$), we find

$$\tilde{X} = \left[F_{10}\frac{\operatorname{ch} Y_0}{\operatorname{sh} Y_0}\frac{e^{-jb_1q}-1}{b_1} + F_{20}\frac{\operatorname{sh} Y_0}{\operatorname{ch} Y_0}\frac{e^{-jb_2q}-1}{b_2}\right]e^{-jkz},$$

$$\tilde{Y} = j\left[F_{10}\frac{\operatorname{sh} Y_0}{\operatorname{sh} Y_0}\frac{e^{-jb_1q}-1}{b_1} + F_{20}\frac{\operatorname{ch} Y_0}{\operatorname{ch} Y_0}\frac{e^{-jb_2q}-1}{b_2}\right]e^{-jkz}, \tag{5}$$

$$F_1 = F_{10}\left[1+\frac{\operatorname{sh} 2Y_0}{\operatorname{sh}^2 Y_0}\frac{1+jb_1q-e^{jb_1q}}{b_1}\right] + 2F_{20}\frac{\operatorname{ch} 2Y_0}{\operatorname{sh} 2Y_0}\frac{(b_1-b_2)e^{jb_1q}-b_1e^{j(b_1-b_2)q}-b_2}{b_1b_2(b_2-b_1)},$$

$$F_2 = F_{20}\left[1+\frac{\operatorname{sh} 2Y_0}{\operatorname{ch}^2 Y_0}\frac{1+jb_2q-e^{jb_2q}}{b_2}\right] + 2F_{10}\frac{\operatorname{ch} 2Y_0}{\operatorname{sh} 2Y_0}\frac{(b_2-b_1)e^{jb_2q}-b_2e^{j(b_2-b_1)q}+b_1}{b_1b_2(b_1-b_2)}. \tag{6}$$

Under antiphase initial excitation of the CTL ($E_{20} = 0$), with $b_1 = 0$, we find

$$F_1 = F_{10}\left(1+q^2\frac{\operatorname{sh} 2Y_0}{2\operatorname{sh}^2 Y_0}\right) \tag{7}$$

$$F_2 = 2F_{10}\frac{\operatorname{ch} 2Y_0}{\operatorname{sh} 2Y_0}\frac{e^{jb_2q}-jb_2qe^{-jb_2q}-1}{b_2^2}. \tag{8}$$

If high-frequency signals from the outputs of both periodic structures (cf. (1) where $y = \pm a$) are added in antiphase, then only the field of antisymmetrical wave E_1 is isolated; an expression for it (cf. relationship (7)) when $Y_0 > 0$ coincides with the corresponding formula for an ordinary traveling wave magnetron-type tube (TWMT); while at $Y_0 < 0$ for a TWMT with positive cold cathode (coupled type of interaction [2], pp 471-481*).

In the case of synphase excitation ($E_{10} = 0$) at $b_2 = 0$, we find an expression derived from (7) and (8) by substituting $E_1 \to E_2$; $b_2 \to b_1$; $\operatorname{sh} 2Y_0/\operatorname{sh}^2 Y_a \to \operatorname{sh} 2Y_0/\operatorname{ch}^2 Y_a$; furthermore, if output signals are composed in phase, formulas similar to those of TWMT theory with one delay system are also derived.

In the case that only one periodic structure is excited, e.g., upper ($E_x(-a) = 0$, $E_x(a) = E_x^+$, cf. (1)), then $F_{10} = F_{20} = F_0/2$ and if $b_1 = -b_2 = b$, one may derive the following estimated relationship for F^+:

$$F^+ \sim F_0\left[1+\frac{q^2}{2}e^{i(\gamma_1-\gamma_2)}\frac{\sin^2(bq/2)}{(bq/2)^2}(1+f)\right]. \tag{9}$$

In deriving (9), it was assumed for simplicity that $K_1 \simeq K_2$, $\operatorname{sh} Y \simeq \operatorname{ch} Y \simeq eY/2$. From the latter formula follows the pulsating nature of the high-frequency field, which is associated with periodic transfer power between structures.

The particular cases considered above at the estimate level show that within the assumptions made, the use of CTL in the traditional circuit of a TWMT amplifier, in linear mode, does not lead to improved efficiency of interaction (non-linear operating mode of TWMT with CTL will be examined below). Furthermore, without calculations it is clear that limiting efficiency of the device should be reduced in comparison with an ordinary TWMT, since the beam must be situated in the interaction space above plane $Y_0 = 0$.

Let us consider the case where electron flux interacts with CTL fields in plane $Y_0 = 0$.

In antiphase excitation, from relationships (5)-(7) we derive the following expressions:

$$X = \frac{F_{10}}{\operatorname{sh} Y_a}\frac{e^{-ibq}-1}{b_1}e^{-iz_0}, \quad Y = 0, \tag{10}$$

*Remember that in this case, coupling resistance is defined in plane $y = a$.

(11) $$F_1 = F_{10}.$$

(12) $$F_2 = \frac{2F_{10}}{\operatorname{sh} 2Y_0} \frac{(b_2 - b_1)e^{jb_1\varphi} - b_2 e^{j(b_2-b_1)\varphi} + b_1}{b_1 b_2 (b_2 - b_1)}.$$

From (10) it follows that within the assumptions made, in this system there occurs only longitudinal grouping of electrons; optimum conditions of grouping correspond to $b_1 = 0$. A similar effect, apparently, can be wisely used to create effective bunchers in which the grouping process is not accompanied by a great loss of potehtial electron energy**. At $Y_0 = 0$, $F_{10} = 10$ (synphase excitation) and $b_2 = 0$, the following relationships occur:

$$X = 0, \quad Y = \frac{F_{10}q}{\operatorname{ch} Y_0} e^{-jz_0},$$

$$F_1 = \frac{2F_{10}}{\operatorname{sh} 2Y_0} \frac{-e^{jb_1\varphi} + jb_1 q e^{jb_1\varphi} + 1}{b_1^2}$$

$$F_2 = F_{20}.$$

Thus, within the applicability of estimates, electrons have only transverse displacements; the degree of grouping is identical for electrons having $Y > 0$ and $Y < 0$. Thus, on the average, the electron beam does not lose potential energy in the high-frequency field, indicating the possible creation of an effective buncher in this case as well.

Some results of solving system of equations (3)-(4) in linear approximation under initial conditions $\tilde{X}(0)$, $\tilde{Y}(0) \neq 0$ $F_{10} = F_{20} = 0$ are cited in study [3], in which is shown the possible creation of effective noise transformers containing CTLs for flux in crossed fields.

3. BASIC NON-LINEAR EFFECTS

Below we will consider basic findings obtained as a result of numerical solution of system of equations (3)-(4) using computers.

**Calculations considering the effect of space charge forces within the model of an infinitely-thin beam, similar to that done in [2] (Ch. V), showed that transverse high-frequency displacements of electrons due to the action of space charge forces are partially equalized by opposing displacements which occur under the influence of the field of the synphase wave E_2, defined by formula (12).

a. A TWMT amplifier using CTL ($F^+(0) = F_0$, $F^-(0) = 0$, $b_1 = -b_2$). Amplitude distribution of the high-frequency field along the length of the interaction space is shown in Figure 2. Strong pulsations $|F^+|$, $|F^-|$ are connected with the process of spatial frequency beating in the CTL. Consequently, electron flux alternately participates in regular or coupled forms of interaction.

Let us touch upon the physical interpretation of processes taking place in greater detail.

At small values of q there occurs an ordinary mechanism of grouping of electron flux in crossed fields (Fig. 2b). Then the grouped electron flux falls into a high-frequency field of different polarization, corresponding to the coupled kind of interaction (Fig. 2c). The grouping process continues, but the cluster begins to drop away from the plane $Y_0 = 0$ and the amplitude of the high-frequency fields diminishes. Later the electron flux again falls in the field of initial polarization, but now in its accelerative phase; degrouping of the cluster starts and the cluster continues to fall away (Fig. 2d). The remaining portion of the cluster falls into the retardation phase of the high-frequency field, leading to a rise of electrons, grouping, and increase of the high-frequency field (Fig. 2e, f). During the rise phase, electrons are able to get rather close to the delay systems. Thus when the cluster of electrons returns to the accelerative phases of the high-frequency field, first participating in coupled and then in the regular kind of interaction (Fig. 2g, h), the processes of energy exchange occur so intensively that amplitudes $|F^+|$ and $|F^-|$ virtually disappear (Fig. 2a, $q = 9.6$). Subsequently the grouped beam induces a high-frequency field in the system which corresponds to the ordinary kind of interaction; and a process similar to that depicted in Figure 2f begins. At such lengths of interaction space, electrons are already starting to settle into periodic structures.

If electron flux is in synchronism with one of the normal CTL waves, for example with wave E_1 ($b_1 = 0$), then the nature of the interaction process changes and will be similar to the corresponding processes in an ordinary TWMT. Let us emphasize once more that the chief distinctions between the processes described and similar ones in type O interaction (cf. chapter I of study [4]) are that the beam in crossed fields participates in both ordinary and coupled kinds of interaction.

b. Grouping of electron flux in CTL fields. From estimated formulas (10)-(12) it follows that condition $F_2 = 0$ corresponds to an ideal buncher.

Let us analyze several factors which significantly alter the process of ideal grouping in non-linear conditions.

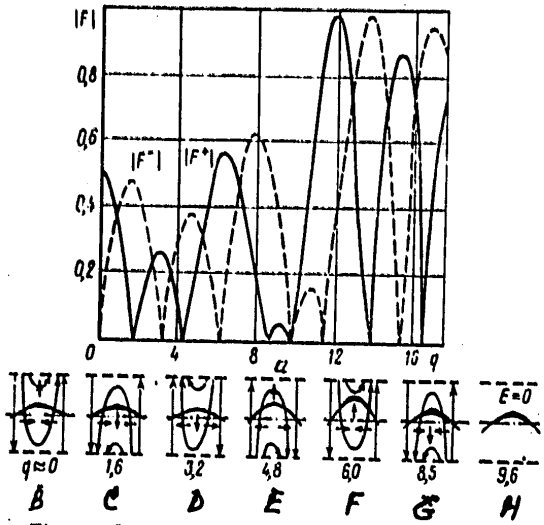

Figure 2. Distribution of amplitudes of high-frequency field in planes of upper |F+|(solid lines) and lower |F-|(dotted) periodic structures (a) and typical form of electron flux in different segments of interaction space (b-d) for the case where input signal is fed to the upper periodic structure ($F_{0+} = 0.5$, $F_{0-} = 0$; $Y_0 = 0$).

If special measures are not taken to suppress wave E_2 through the interaction space, there is some intensification of wave E_1 up to and including saturation; the level of saturation weakly depends on the input signal level (Fig. 3a). Electrons in this case have both longitudinal and transverse displacements; the electron cluster remains immobile with respect to wave E_1, always located in its retardation phase, and breaks down into two virtually symmetrical portions, one of which rises upward from Y = 0, while the other falls (Fig. 3b); at some length, electrons begin to settle into periodic structures. This type of grouping is linked with the existence of wave E_2 (hatched curves in Figure 3a), which is excited in phase with the cluster and remains almost synchronous with it, but slightly advanced in phase, virtually until the settling process begins (hatch-dotted line in Figure 3a). The most significant distinction of this buncher from an ideal one is that in the nascent inclined clusters, electrons are concentrated not in plane Y = 0, but in regions of maximum transverse displacements of electrons (vertical displacements may be reduced by increasing b_2, or by using special "electrodynamic" means to attenuate the field of symmetrical wave E_2 and, as was noted, space charge forces should lead to a reduction in transverse displacements of electrons).

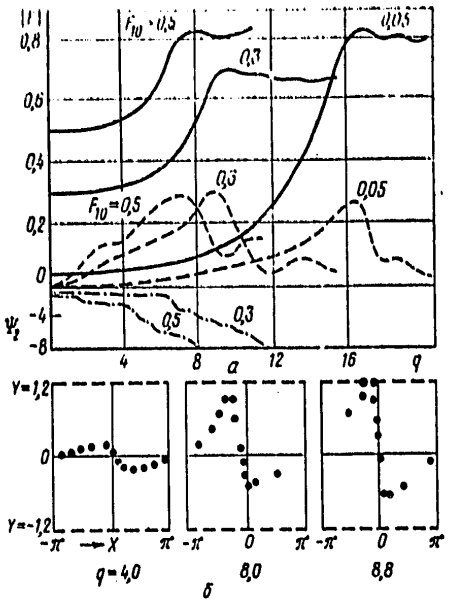

Figure 3. Distribution of amplitudes of high-frequency field of antisymmetrical $|F_1|$ (solid lines) and symmetrical $|F_2|$ (dotted lines) waves and phase of symmetric wave Ψ_2 (hatch-dotted) (a) and position of individual electrons during one period of high-frequency field E_1 in different segments of interaction space (b) for the case where an antisymmetrical wave ($F_{10} \neq 0$, $F_{20} = 0$; $b_1 = 0$, $b_2 = -2$; $Y_0 = 0$) is excited at the input.

If the electron flux in static state is situated below plane Y = 0, then there begins to appear a mechanism of coupled interaction: sequential processes of grouping and ungrouping of electron flux take place, accompanied by a reduction or increase in amplitude of field $|F_1|$ (Fig. 4a, b; with value of Y_0 chosen for calculation, nature of bundle grouping does not differ greatly from the case $Y_0 = 0$).

In a bundle for which $Y_0 > 0$, the mechanism of ordinary interaction in crossed fields occurs: both the number of electrons having positive transverse high-frequency displacements and the amplitude of these displacements increase; a more rapid increase of amplitudes of both field waves occurs than in the cases examined.

Analysis of the buncher in which the input signal excites symmetrical wave E_2 showed that, as was done from estimates, the potential energy of the beam changes slightly and the high-frequency field remains almost constant at large input signal values (Fig. 5a, b).

These results permit us to conclude that with the aid of a buncher containing CTL, it is possible to shape rather dense clusters. The use of this buncher as an input section in instruments having crossed fields may significantly improve the characteristics of the latter. Corresponding calculations show that efficiency may be increased by 10-15%. The possibility of considerable truncation of the length of the input section (by 2 to 2.5 times) in comparison with an ordinary TWMT is most interesting; it is very important for the improvement of device resistance to parasitic self-excitation.

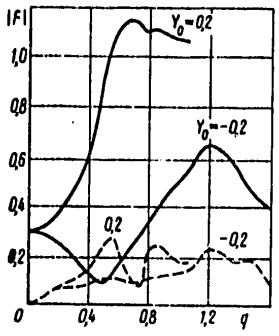

Figure 4. Distribution of amplitudes of high-frequency field of antisymmetrical $|F_1|$ (solid lines) and symmetrical $|F_2|$(dotted lines) waves with asymmetrical positioning of electron flux ($Y_0 \neq 0$) for the case where an antisymmetrical wave is excited at the input ($F_{10} = 0.3$, $F_{20} = 0$; $b_1 = 0$, $b_2 = -2$).

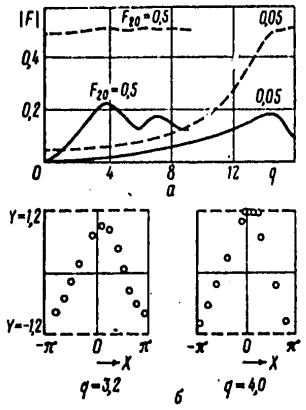

Figure 5. Distribution of amplitudes of high-frequency field of antisymmetrical $|F_1|$ (solid lines) and symmetrical $|F_2|$(dotted) waves (a) and position of individual electrons during one period of HF field E_2 in different segments of interaction space (b) for the case where a symmetrical wave is excited at the input ($F_{10} = 0$, $F_{20} \neq 0$; $b_1 = 2$, $b_2 = 0$; $Y_0 = 0$).

CONCLUSION

The results cited above supplement the known picture of physical processes of interaction in crossed fields and indicate the theoretical possibility of creating beam-type type-M devices with improved parameters.

In the future it will be important to study the effect of the forces of space charge and cyclotron waves on the nature of multiple-wave interactions in type M beam-type devices.

It is almost obvious, in particular, that explosive instability [5] must occur even in three-frequency interaction in type M beam-type devices when cyclotron waves are excited in the beam.

Experimental verification of the posited effects is especially important.

APPENDIX

Let us note that the problem of an ideal buncher (no losses in potential energy of the HF field) has an analytical solution.

For an antisymmetrical buncher ($F_2 = 0$) where $Y = Y_0$, the solution of equations (3) and (4) appears as

(P1) $$\ln\left|\frac{\mathrm{tg}(X/2)}{\mathrm{tg}(X_0/2)}\right| = -\frac{F_{10}}{\mathrm{sh}\, Y_a}q.$$

For a symmetrical buncher ($F_1 = 0$) where $X = 0$, we may derive

$$\frac{\mathrm{arctg}(\mathrm{sh}\, Y)}{\cos X_0} = \frac{F_{20}}{\mathrm{ch}\, Y_a}q.$$

The right sides of these equations completely determine the degree of grouping of electrons. Let us illustrate this with the derivation of conditions of formation of an "almost point" cluster.

If there are 24 "machine" electrons per period of HF field, then electrons lagging behind electrons which have the phase $\pm\pi$ by an interval $\Delta = 2\pi/24$, will gather in the interval 2Δ around an electron having the phase $X_0 = 0$ (forming an almost point cluster) at length q, which may be defined from (P1). For example, where $Y_a = 1.2$ for $F_{10} = 0.5$ is obtained $q = 12$ (high value of q is linked with fact that D_0 is defined in plane of periodic structures; in "ordinary" definition D_0 is in plane if beam $q = 4.2$).

REFERENCES

1. R. A. Silin, V. P. Sazonov. Delay systems [Zamedlyayushchiye systemy]. Izd. Sovetskoye radio, 1966.

2. V. N. Shevchik, D. I. Trubetskov. Analytical methods of calculation in microwave electronics [Analiticheskiye metody rascheta v elektronike SVCh]. Izd. Sovetskoye radio, 1970.

3. Ye. P. Bocharov, D. I. Trubetskov, V. P. Shakhin. RADIOTEKHNIKA i ELEKTRONIKA, 1976, 21, 12, 2358.

4. D. V. Sokolov, D. I. Trubetskov, Yu. P. Sharayevskiy, V. P. Shakhin. RADIOTEKHNIKA i ELEKTRONIKA, 1978, 23, 8, 1678.

5. M. I. Rabinovich, IZV. VUZOV MVSSO SSSR (Radiofizika), 1974, 17, 4 494.

8617
CSO: 1870

ELECTRONICS AND ELECTRICAL ENGINEERING

SIGNAL DETECTION ON CRT AGAINST NOISE BACKGROUND: NONPARAMETRIC MODEL

Moscow RADIOTEKHNIKA i ELEKTRONIKA in Russian No 11, Nov 78 pp 2439-2442

[Article by V. N. Budko, F. M. Klement'yev, N. M. Novikova: "Nonparametric model of detection of signals observed by human operator on CRT against a background of noises"]

[Text] For efficient operation of radio engineering systems in which the final link in the processing of information is a human operator, it is necessary to match the working characteristics of the systems and man. One vital issue of such coordination is that of a formalized description of human behavior in visual detection of signals against a background of noises on a CRT. Let us consider in the general form those processes which make up the foundation of psychological data in describing the situation of detection of signals by a human operator. Let there exist some set of signals S, which in some form is depicted as a set of mental images. Let us assume that there exists some solving device which, on the basis of extant sensory data, works out a set of response reactions or behavioral forms. In addition to the set of external signals there also exist sources of additional external information. Naturally, output information linked with the results of response reactions in the form of feedback enters the input of the operating sensory system. Signals of feedback may be changes in the environment or information about evaluation of results of actual behavior of the human operator. There exists a source of internal information which units various systems associated with the work of the regulatory, predictive, and an especial motivational-estimational mechanism. Both sources of external information and sources of internal information affect the work of the decision unit. Thus the working characteristics of the human operator who detects a signal against a background of noises on the CRT has a probability nature. Working characteristics we take to mean the relationship of probability of detection of a signal and its intensity when the latter is observed on a background of noise.

The fundamental probability set of working characteristics of a human operator is generated by the following features: 1) fluctuation of sensory threshold; 2) probability characteristics of external effects; 3) straying of attention; 4) lack of observation time due to finite speed of information handling; and 5) signal masking by noise.

We use the operational definition of threshold as some empirical quantity applicable for the characteristics of functional possibilities of man [1]. The actual working characteristics of the human operator are the result of an integrative action of the sources of the probability set mentioned above. To explain the logical foundation of work of the decision unit, and the logical behavioral basis of the human operator in the situation of detecting signals against a noise background on a CRT, it is necessary to eliminate the effect of the aforementioned causes on the work of the human operator. Actual working characteristics of the operator can be experimentally obtained allowing for the requirements stated above.

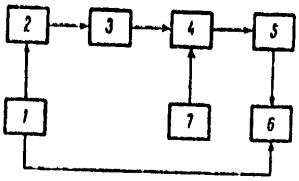

Figure 1. Block diagram of connection of devices.

The block diagram of connection of devices for the experiment is shown in Figure 1.

A trigger pulse from a synchronizer 1 produces simultaneous turn on of the display scanner 6 and the pulse shaper 2. An oscillograph type C8-9A with memory is used as the display. A U-pulse generator is employed as the pulse shaper. The U-shaped pulse obtained at the shaper output is transformed by filter 3 into a bell-shaped pulse and enters the adder 4, where there is additive summation with low-frequency noise (normally distributed) which enters from the noise generator 7. After passing through a matching filter 5, the signal+noise mixture is fed to the oscillograph screen 6. The screen shows the realization of the mixture of bell-shaped pulse with normal low-frequency noise. The signal is chosen with rather high intensity to eliminate the effect of sensory threshold fluctuations. To avoid having a priori information (as an additional information source) display a probability nature, the signal was always situated at the same point on the scanning line: this was known to the operator. In the realization being presented, the signal was not always present, but only in 5/6 of the cases. Alternation of blank (noise only) and signal (signal+noise) realizations with different signal amplitudes was done in random sequence.

The methods used in working with operators who participated in the experiment were as follows: the human operator was given the task of detecting a signal presented as a one-time display of signal and noise mixture. The display observation time was unlimited, i.e., the human operator had not information handling time deficit. The brightness of the scanning line during the experiment was kept constant; before the start of the experiment the operator became adapted to this brightness. Experiments were run in a darkened room with no exterior illumination of the screen. The operator's reactions contained two responses: "yes"--there is a signal, and "no"--there is no signal. Operator responses were evaluated by a value matrix: reward for correct detection and fine for erroneous decision. Errors were signals missed and false alarms--detection of a signal when only noise was displayed. Operators first took part in control experiments and were trained. When the results of the operators became stable, they switched to the basic experiments.

Each series of experiments lasted an hour or less to eliminate fatigue of the visual analyzer and straying of operator attention.

The probability of signal detection, and the probability of false alarm, were evaluated according to the frequency of the event being evaluated:

$$p = N_1/N,$$

where N_1 is the number of positive decisions; N is the total number of displays; in experiment N = 100 for each signal-to-noise ratio.

Four trained operators participated in the experiment; each received a working characteristic; the averaged working characteristic curve is shown in Figure 2.

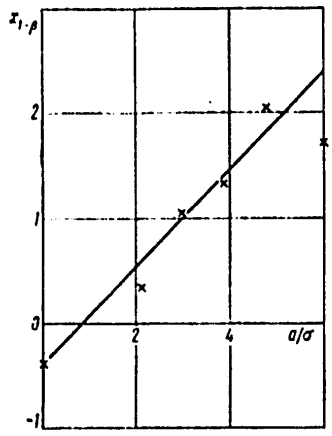

Figure 2. Working characteristic of mean statistical worker.

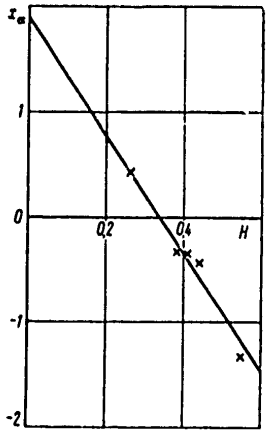

Figure 3. False alarm probability versus coefficient H.

In this figure, the x-axis contains the plots of the probability of correct detection in quantiles of normal distribution; along the y-axis is plotted the signal-to-noise ratio. The operator's working characteristic in this system of coordinates is represented by a straight line:

(1) $$x_{1-\beta} = x_a + a/H,$$

where $x_{1-\beta}$ is the probability of correct detection in quantiles of normal distribution; x_a is the probability of false alarm in quantiles of normal distribution with zero signal amplitude; a/ is the signal-to-noise ratio. H is some coefficient which is typical of the human operator.

According to the χ^2 principle, one may claim that the points lie along a straight line with 0.99 probability (1).

Coefficient H may be computed for each operator by using his actual working characteristic obtained in our experiment.

A simple relationship, shown in Figure 3, was found between coefficient H and the probability of false alarm x_a; the probability of false alarm x_a is plotted along the x-axis in quantiles of normal distribution, and the coefficient H is plotted on the y-axis.

By using the χ^2 principle, we can state that the points lie on a straight line with a probability of 0.99.

Under the conditions of our experiment, the relationship between H and x_a is expressed by an equation of the type

(2) $$H = -0.17x_a + 0.32.$$

By substituting (2) in (1), we derive an expression for the working characteristic of the mean statistical operator, where the parameter describing the individual nature of the operator will only be the probability of false alarm x_a.

Let us examine the working characteristics of automatic non-parametric signal detectors and compare them with the working characteristics of the human operator obtained in our experiment.

A signal detector is called non-parametric if it provides constant probability of false alarm with very weak limitations on the statistical characteristics of input signals [2]. The working characteristics of automatic nonparametric detectors used for signal detection are the sign, rank, and sign-rank statistics cited in [2]. They have identical structure and may be generalized and represented as follows:

(3) $x_{1-\beta} = x_{\alpha} + n/\sigma K,$

where K is some coefficient, distinctive for different working characteristics, depending on the kind of signal and the distributive function of interference. Generalized formula (3) and the working characteristic of the mean statistical operator (1) have identical structures. This also suggests that in detection of signals with background noise on a CRT, the human operator appears to use non-parametric criteria since the results of his work can be represented in a form analogous to (3).

A distinctive feature of non-parametric detectors is the independence of the probability of false alarm on the kind of noise distribution function.

For the human operator, this peculiarity was tested experimentally. The working characteristics were recorded for the same four trained operators for two different noise distribution functions. Within the limits of reliable interpretation of error, the probability of false alarm was almost unchanged. The supposition of non-parametric criteria used by the human operator in signal detection with background noise on a CRT will aid in calculating the efficiency of operation of the "man-CRT" system.

REFERENCES

1. K. V. Bardin. Problems of sensitivity threshold and psychophysical methods [Problema porogov chuvstvitel'nosti i psikhofizicheskiye metody], Izd. Nauka, 1976.

2. B. R. Levin. Theoretical bases of statistical radio engineering [Teoreticheskiye osnovy statisticheskoy radiotekhniki], 3, Izd. Sovetskoye radio, 1976.

8617
CSO: 1870

ELECTRONICS AND ELECTRICAL ENGINEERING

SIDE-LOBE FILTERS FOR PHASE-MANIPULATED SIGNALS

Moscow RADIOTEKHNIKA i ELEKTRONIKA in Russian No 11, Nov 78 pp 2442-2445

[Article by V. P. Ipatov: "On side-lobe suppression filters for periodic phase-manipulated signals"]

[Text] The theoretical possibility of total suppression of all side-lobes of a periodic reciprocal correlation function (PRCR) of a phase-manipulated signal and mirror pulse response of a linear filter is shown in study [1]. In [2] it was established that a necessary and adequate condition for the existence of such a filter (side-lobe suppression filter: SLSF) is the linear independence of all cyclical shifts of the periodic phase-manipulated (PPM) signal. Relationships cited in [2], which connect the structure and indicator of SLSF with the periodic autocorrelation function (PACF) are convenient for synthesis of SLSF for signals with relatively simple (for example, one level [3]) PACF. In the same cases where the form of PACF was not previously specified, especially in synthesis of the PPM-signal/SLSF pair, it can be more preferable to have expressions obtained below with the aid of a discrete Fourier transformation (DFT).

As in [2], let $x_0, x_1, \ldots, x_{N-1}$ be a sequence of complete amplitudes of a PPM signal of period N; to the j-th cyclical shift of the signal x_j, $x_{((1+j))}, \ldots, x_{((N-1+j))}$, where $((k)) \equiv k \pmod N$, $0 \leqslant ((k)) \leqslant N-1$ corresponds an N-dimensional vector-column (hatched line designates transposition):

$$X_j = \|x_j, x_{((1+j))}, \ldots, x_{((N-1+j))}\|.$$

Furthermore, let

$$E = \sum_{i=0}^{N-1} |x_i|^2$$

be the energy of one period of a PPM signal.

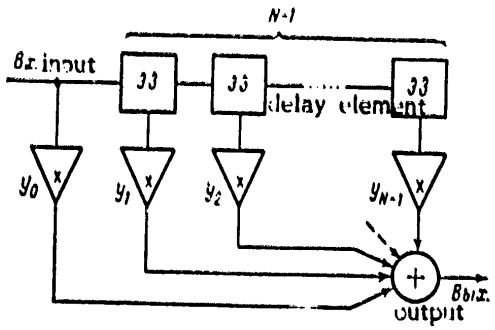

Transversal SLSR of PPM signal

Let us introduce an NxN matrix

$$A = ||X_0, X_1, \ldots, X_{N-1}||'$$

and write out a correlation matrix of cyclical shifts of a signal $B = ||(1/E)(X_i, X_j)||$, where (X_i, X_j) is the scalar product of vectors X_i and X_j in the form (asterisk designates transposition with complex conjugation)

(1) $$B = \frac{1}{E} AA^*.$$

The block diagram of an SLSR as a transversal filter [4] is shown in the figure, where ЭЗ is an element of delay by the duration of the discrete of a PPM signal, and $y_0, y_1, \ldots, y_{N-1}$ is a sequence of weight coefficients which can be seen as components of an N-dimensional vector-column of the filter

$$Y = ||y_0, y_1, \ldots, y_{N-1}||'.$$

Complex amplitudes z_i, $i = 0, N-1$ at the filter output may be derived by periodic (circular) convolution [5] of the sequences x_i, y_l, $l = \overline{0, N-1}$

(2) $$z_t = \sum_{l=0}^{N-1} x_l y_{((t-l))} = \sum_{l=0}^{N-1} x_{((t-l))} y_l, \quad t = \overline{0, N-1}.$$

By assuming in conformity with the filter designation $z_i = 0$, $i = \overline{1, N-1}$, $z_0 = a$, where a is an arbitrary complex number not equal to zero, and by introducing a DFT of the sequence z_i

$$c_k = \sum_{t=0}^{N-1} z_t \exp\left(-jk\frac{2\pi}{N}t\right), \quad k = \overline{0, N-1},$$

we find that

(3) $$\xi_k = a, \quad k = \overline{0, N-1}.$$

Now applying to (2) the theorem of circular convolution [5] allowing for (3), we arrive at

(4) $$\eta_k = \frac{a}{\xi_k}, \quad k = \overline{0, N-1},$$

where

$$\xi_k = \sum_{i=0}^{N-1} x_i \exp\left(-jk\frac{2\pi}{N}i\right), \quad \eta_k = \sum_{i=0}^{N-1} y_i \exp\left(-jk\frac{2\pi}{N}i\right), \quad k = \overline{0, N-1}$$

is the DFT of the sequences x_i and y_i.

The cited relationship proves that for the existence of a SLSR is necessary and adequate a distinction of all components of the signal DFT from zero, i.e., the satisfaction of N inequalities

(5) $$\xi_k \neq 0, \quad k = \overline{0, N-1}.$$

The latter condition is identical to the condition of linear independence of all cyclical shifts of the PPM signal

(6) $$\det A \neq 0.$$

Actually, (6) only takes place when all intrinsic values of A are not zero. But since the A matrix is a circulant [6], its intrinsic values are equal to ξ_k, $k = \overline{0, N-1}$ and thus (6) follows from (5) and vice versa.

As seen in (4), the SLSR converts the spectrum (in the sense of the DFT) of a PPM signal into a uniform one and thus may be called a discrete Urkowitz filter [7].

To derive the weight coefficients of the SLSR it suffices to switch to an inverse DFT in (4)

$$(7) \qquad y_t = \frac{1}{N}\sum_{k=0}^{N-1}\eta_k \exp\left(jk\frac{2\pi}{N}t\right) = \frac{a}{N}\sum_{k=0}^{N-1}\frac{\exp\left(jk\frac{2\pi}{N}t\right)}{\xi_k}, \quad t=\overline{0,N-1}.$$

Let us now define the signal-to-noise ratio for a primary lobe at the output of a SLSR $q^2 = |a|^2/Y^*KY$, where K denotes the correlation matrix of input noise. If the latter is stationary and correlation time does not exceed the duration of the discrete of the PPM signal, $K = \sigma^2 I$, where σ^2 is average power of noise, I is the unitary matrix. Then on the basis of (7)

$$Y^*KY = \sigma^2 Y^*Y = \sigma^2\sum_{t=0}^{N-1}|y_t|^2 = \frac{|a|^2}{N}\sigma^2\sum_{k=0}^{N-1}|\xi_k|^{-2},$$

$$q^2 = (N/\sigma^2)\sum_{k=0}^{N-1}|\xi_k|^{-2}.$$

Not only does the quantity q^2 represent basic interest, but losses of the SLSR in the signal-to-noise ratio as compared with the matching filter of a photon counter. In describing them, as in [2] (with accuracy to denotations), by the number $\nu = q^2/q_0^2$, where $q_0^2 = E^2/X^*KX$ is the signal-to-noise ratio for the primary lobe at the output of a photon counter, we have for earlier assumptions with respect to $KX^*KW = \sigma^2 E$, and

$$(8) \qquad \nu = \frac{N}{E\sum_{k=0}^{N-1}|\xi_k|^{-2}}.$$

Since the B matrix is a circulant (cf. (1)), whose lines are cyclical permutations of the PPM signal PACF, its intrinsic values are components of the DFT of the PACF, i.e., $|\xi_k|^2/E$, $k = \overline{0, n-1}$. Due to the symmetricity of B, the intrinsic values of the inverse matrix B^{-1}, which always exist when (5) is valid (SLSR exists), are equal to $E|\xi_k|^{-2}$. Thus (8) can be represented as

$$\nu = N/S_n B^{-1}$$

where $\mathrm{Sp}B^{-1}$ is the trace of matrix B^{-1}.

Relationships (7),(8) may be extremely useful in solving problems of SLSF synthesis and the PPM-signal pair (especially, a binary PPM signal) with the SLSR using computers: they require much lower expenditures of machine time as compared to data obtained in [2]. Actually, computation of elements of the Gram determinant for deriving φ according to [2] requires execution of $N^2/2$ operations of multiplication of complex numbers. To expand the determinant by reduction to triangular form requires another $(N+1)(N(N-1)/3$ such operations. In sum, computation time for on computer for large N is proportional to the quantity $N^3/3$, since multiplication usually occupies the overwhelming part of computer time. At the same time, the use of (8) even in direct realization of the DFT algorithm permits us to save time proportional (where $N \gg 1$) to N^2 (N^2 operations of multiplication of complex numbers to compute all ξ_k and N computations of the square of the modulus of ξ_k). This gain in expenditures of computer time may be increased many times by using known algorithms for rapid Fourier transformation [4, 5].

REFERENCES

1. Questions of statistical theory of radio location [Voprosy statisticheskoy teorii radiolokatsii], ed. by G. P. Tartakovskiy, II, Izd. Sovetskoye radio, 1964.

2. V. P. Ipatov, RADIOTEKHNIKA i ELEKTRONIK,1977, 22, 8, 1600.

3. M. B. Sverdlik. Optimum discrete signals [Optimal'nyye diskretnyye signaly], Izd. Sovetskoye radio, 1975.

4. Introduction to digital filtration [Vvedeniye v tsifrovuyu fil'tratsiyu] ed. by R. Bogner and A. Konstantinidis, Izd. Mir, 1976.

5. B. Gold, Ch. Raider. Digital processing of signals [Tsifrovaya obrabotka signalov]. Izd. Sovetskoye radio, 1973.

6. R. Bellman. Introduction to the theory of matrices [Vvedeniye v teoriyu matrits]. Izd. Nauka, 1976.

7. H. Urkowitz. Filters for Detection of Small Signals in Clutter, J. Appl. Phys., 1953, 24, 1024.

8617
CSO: 1870

ELECTRONICS AND ELECTRICAL ENGINEERING

AMPLIFICATION OF WIDE-BAND SIGNALS IN TYPE O TRAVELING-WAVE TUBES

Moscow RADIOTEKHNIKA i ELEKTRONIKA in Russian No 11, Nov 78 pp 2455-2458

[Article by B. Ye. Zhelezovskiy, Ye. Ye. Zhelezovskiy, R. N. Karimov, Yu. V. Klinayev: "Study of Aspects of Amplification of Wide-Band Signals in Type O Traveling-Wave Tubes with Random Oscillations"]

[Text] Amplification of noise-type oscillations (cf. [1,2,3]) is employed in the operation of some electronic devices and radio engineering systems in microwave technology. In this respect, the greatest interest is involved with wide-band amplifiers, especially type O and M traveling-wave tubes.

Ordinary amplification of a noise-type signal in a traveling-wave tube (TWT) is associated with its direct action on the input of the delay system. As far as the authors know, theoretical analysis of noise-type signal amplification in TWTs has only been done for M-type devices [4].

In this study, a similar approach has been taken toward TWTs. The investigation was mainly aimed at explaining the amplification efficiency of noise-type signals in TWT with various methods of insertion into interaction space.

The method of investigation of noise-type signal amplification employed is a realization of a stationary normal random process and is based on the notion that it is formed by the harmonics of various frequencies. It is clear that a random process has no determinate harmonic components, but it makes it possible to formally carry out Fourier analysis and compute the spectral components. Evaluation of the spectral density of noise-type signals is inconsistent, but a smoothed evaluation will be suited for practical applications. To obtain consistent statistical evaluations, it is necessary to smooth out the spectral sampling density in terms of a set of segments of realization of noise-type signals or in terms of frequencies [5].

Furthermore, a spectral description of a noise-type signal is convenient for shaping realizations of pre-set spectral density.

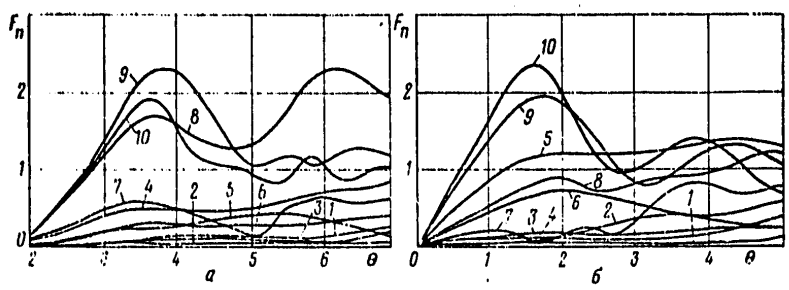

Figure 1. Distribution of amplitudes of noise-type signal components through length of interaction space with: (a) insertion of signal to input of delay system; (b) insertion of signal via electron flux.

Nonlinear equations of multiple-frequency interaction of electron flux with a direct electromagnetic traveling wave were utilized in calculations. Calculations were carried out according to known equations described, for example, in [6].

In determinacy computations it was assumed that the delay system of a traveling-wave tube has an octave bandpass and delay and coupling resistance are constant in this band. The effect of attenuation, the action of space charge forces and the interaction beyond the limits of the band with double overlap in frequency were not taken into account. The case of a thin beam with synchronism of electron flux with a traveling electromagnetic wave was investigated. Calculations were carried out for equidistant spectra, simulated by ten components with a ratio of extreme spectral frequencies to the fundamental frequency of the working equations equal to 9 and 18, respectively. The quantities of initial amplitudes of the spectral components with the interaction of a noise-type signal on the input of the delay system and the quantities of amplitudes of high-frequency fields which modulate the electron flux at the input into the interaction space (with signal insertion via electron flux) were obtained by repeated multiplication by a norming multiplier of random numbers from the set with normal distributive law having parameters (0.1), and quantities of initial phases--from a set of random numbers with uniform distribution in the interval $(-\pi,\pi)$. Each realization differed in quantity and phase of each spectral component. Furthermore, the dispersion of normal and the distributive interval of uniform random numbers did not vary from spectrum to spectrum. The values of the norming coefficients for normal random numbers were selected as equal to 0.02. The amplification parameter was taken as equal to 0.05. The number of electrons per period of fundamental freuqenecy was chosen as equal to 288. For each of the two methods of insertion of the noise-type signal (directly into the input of the delay system and via electron flux) into the interaction space of the traveling-wave tube, 10 realizations of the random process were investigated.

The nature of gain of spectral components of the individual realization is illustrated in Figure 1. In it is shown the distribution lengthwise in the interaction space of the traveling-wave tube of amplitudes of components of the high-frequency field with insertion of a noise-type signal into the input of the delay system (Fig. 1a) and by means of pre-modulation of electron flux. Numeration of curves in the figures corresponds to the order number of the component of the equidistant spectrum used in calculations. The distinctive behavior of relationships at initial sections of the interaction field and at the point of maximums of the component fields is clearly seen in the figures.

The behavioral nature of the curves, as a rule, corresponds to the patterns of signal gain in the multiple-frequency operating mode of a traveling-wave tube: spectral components with greatest values of input signal amplitudes are amplified usually to greater output amplitudes; excitation of intensive harmonics of low-frequency components of the spectrum is observed (especially with small interaction space lengths); phase relationships play a major role in the amplification process; one may see suppression of individual components, especially those having small input signal amlitudes, and so forth.

In Figure 2 is shown the lengthwise distribution of traveling-wave tube interaction space of the total high-frequency power for various realizations. As an example is given the power distribution of five realizations with insertion of a noise-type signal directly into the input of the delay system (Figure 2a) and via electron flux (Figure 2b). One can see the unified pattern of behavior of relationships for individual realizations. The first peak is associated with the prefered amplification of one or more (most often, high-frequency) components of the octave spectrum. The second peak is due (with greater length of delay system) to the more uniform amplification of diverse components. The quantity and location of the power peaks themselves differ for individual realizations and reflect the change in power from realization to realization. Naturally, when the noise-type signal is inserted via electron flux, the output power has peaks with shorter lengths of the delay system, and the difference in size of the peaks themselves is barely related to the method of signal insertion into the traveling-wave tube.

In Figure 3 are shown the mean statistical relationships obtained by averaging according to realizations. Curve 1 of Figure 3 depicts the lengthwise distribution of traveling-wave tube interaction space of medium high-frequency output with the influence of a noise-type signal on the delay system input; curve 2--with preliminary noise-type modulation of electron flux. For comparison, in the same figure curve 3 shows the lengthwise distribution of interaction space of a high-frequency power TWT with amplification of a monochromatic signal fed to the delay system input at a frequency equal to the average frequency of the noise-type spectrum. A comparison of relationships proves that with amplification of a wide-band noise-type signal in a TWT, the magnitude of output power is much lower than with amplification of a monochromatic signal. The magnitude of peak output power at the maximum, for the cited relationships with amplification of a noise-type signal, is about 1.3 to 1.4 times lower than in amplification of a harmonic signal. Of course, with the fixed length of a device, the drop in output power may

be more significant. For example, with an interaction space length corresponding to the maximum power of a harmonic signal, the output power of an amplified wide-band noise-type signal is almost halved. Thus, with optimization of TWT design for amplification of a noise-type signal, the basic geometric dimensions of interaction space, and particularly the delay system length, must be selected to allow for random characteristics of the input signal. Additional increase of efficiency may be provided by ordinary methods described, for example, in [6, 7], or by preconceived alteration of input signal parameters.

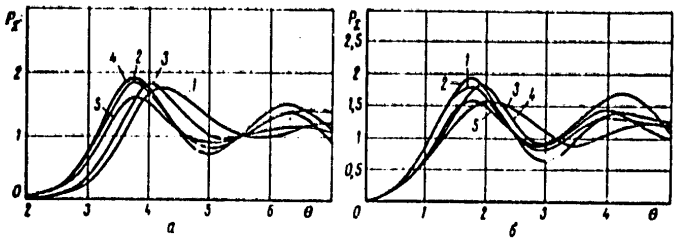

Figure 2. Lengthwise distribution of interaction space of total microwave outputs for five realizations of a noise-type signal where: (a) signal is inserted into delay system input; (b) signal is inserted by means of electron flux.

The proposed methods of analysis and numerical calculations on computer let us evaluate the energy possibilities of TWT with amplification of wide-band noise-type oscillations. Cases of insertion of high-frequency power directly into the delay system and via electron flux were analyzed. The results of computation showed that with amplification of noise-type oscillations in TWT there is a drop in output power as compared with the amplification of monochromatic oscillations; in actual devices, designed for amplification of harmonic signals, this could be extremely significant and could make it necessary to incorporate design changes.

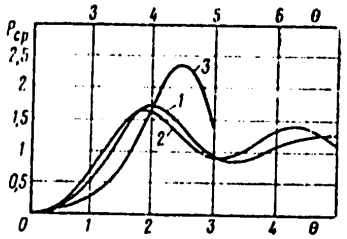

Figure 3. Lengthwise distribution of interaction space of averaged total microwave power where: (1) noise-type signal is inserted into delay system input (upper scale of y-axis); (2) noise-type signal is inserted via electron flux (lower scale of y-axis); (3) harmonic signal is inserted into input of delay system.

REFERENCES

1. Microwave engineering [SVCh-energetika], ed. E. Okress, Izd. Mir, 1971, 1, pp. 113-125.

2. A. M. Fadeyev. Noise radiolocation systems (review), ZARUBEZHNAYA RADIOELEKTRONIKA, 4, 1968.

3. Microwave engineering, op. cit., 3, pp. 100-109.

4. B. Ye. Zhelezovskiy, Ye.Ye. Zhelezovskiy, R. N. Karimov, Yu.V. Klinayev, RADIOTEKHNIKA i ELEKTRONIKA, 1977, 22, 6, 1222.

5. Dzh. Bendat, A. Pirsol. Measurement and analysis of random processes. (Translation from English), Izd. Mir, 1974.

6. A. M. Kats, Ye. M. Il'ina, I. A. Man'kin. Nonlinear phenomena in microwave devices of O type with prolonged interaction [Nelineynyye yavleniya v SVCh-priborakh O-tipa s dlitel'nym vzaimodeystviyem], Izd. Sovetskoye radio, 1975.

7. L. F. Teslenko, A. B. Semenova. Increasing efficiency in O-type traveling wave tubes, OBZORY PO ELEKTRONNOY TEKHNIKE, SERIYA ELEKTRONIKA SVCH, Vyp. 10(325), TsNII "Elektronika", Moscow, 1975.

8617
CSO: 1870

GEOPHYSICS, ASTRONOMY AND SPACE

A SPECIALIZED COMPUTER FOR MARINE DIGITAL GRAVIMETERS

Moscow PRIKLADNAYA GEOFIZIKA in Russian No 88, 1977 pp 102-111

[Article by A. V. Staklo: "A Specialized Computer for Marine Digital Gravimeters]

[Text] Taut-wire gravimeters and accelerometers (4,6), the AMG [automated marine gravimeter] (10) and the TsAG [digital automated gravimeter] (1) belong to the class of marine gravimeter devices having output in digital code form. The last-mentioned device is very advanced. New devices, as per GOST [All-Union State Standard] requirements, are required to have units which permit recording in digital form. In order to reduce the volume of recorded data and the time required for final processing of material on a general-purpose computer and also to provide for convenience in the work of the operator, it is desireable to carry out initial processing of the gravimetric data right at the time of the observation in the ocean.

Basically, initial processing amounts to filtering the signals incoming from the gravimeter. Computing by readouts from the equipment of a sudden increase in the force of gravity is required in addition to the filtering. For the majority of gravimeters, gravitational increments may be defined by the formula (5)

$$\Delta g = k_1 (n - n_0) + k_2 (n - n_0)^2, \qquad (1)$$

where k_1 and k_2 are the gravimeter constants and n_0 and n are the initial and current readouts.

For gravimeters with practically linear characteristics such as the TsAG, $k_2 = 0$.

A filter which makes it possible to separate the signal from the noise in the best way is called an optimum filter. Of the possible criteria of quality for a gravimeter, the most important are filter accuracy, high-speed response, cost and its complexity. In studies (8,9) the characteristics of the output and noise during marine gravimetric surveying are given making it possible to conclude that a filter which is optimum according to the criterion of the

minimum root-mean-square should come close to being an ideal filter for low frequencies having a very steep characteristic slope with a cutoff frequency of approximately 0.003 Hz.

Closest to the ideal filter are the Battervort, the Chebyshev, the elliptical and others. In principle, any of them may be used for solving the problem of separating a gravimetric signal from noise. In practice, filters which have a simpler structure are often used. Multistage filtering with variable cutoff (6) is especially easy to program and requires a small expenditure of machine time.

Let us examine the construction of digital filters from the point of view of the convenience in implementing them in a specialized unit. For a description of digital filters it is convenient to use a z-transform which is a discrete analog Laplace transform (2,7). If the transfer function of the linear system is represented in the form

$$W(s) = \sum_{i=0}^{M} c_i s^i \Big/ \sum_{n=0}^{N} d_n s^n, \quad M < N,$$

then the corresponding discrete transfer function is expressed in general form as follows:

$$W(z) = \sum_{j=0}^{N-1} a_j z^{-j} \Big/ \left(1 + \sum_{j=1}^{N} b_j z^{-j}\right), \tag{2}$$

where $z = e^{sT}$ is the shift in time T statement.

If at least one value b_j is not equal to zero, then the filter in expression (2) is recursive, that is for generating the output signal not only the value of the input signal is used but also the previous value of the output. If all $b_j = 0$ then the filter has a nonrecursive structure and a simple linear weighting of the input readouts is used for generating the output signal.

Nonrecursive filters may have excellent phase characteristics but a large number of sections is required for achieving a sharp cutoff. Filters with a sharp cutoff of the frequency characteristic are easy to design using a recursive structure.

For illustration let us consider the design of a digital Battervort filter. The square of the modulus of the frequency characteristic of this filter is

$$|W(s)|^2 = [1 + (-1)^m (s/\omega_c)^{2m}]^{-1}, \tag{3}$$

where ω_c is the cutoff frequency.

In this case it is convenient to make use of a bilinear z-transform (7) using the substitution

$$s \longrightarrow \frac{1 - z^{-1}}{1 + z^{-1}} \cdot \frac{2}{T}. \tag{4}$$

The transfer function of the required digital filter based on (3) and (4) is

$$W(z) = \left\{1 + (-1)^m \left[\left(\frac{1-z^{-1}}{1+z^{-1}}\right)\Big/\frac{\omega_c T}{2}\right]^{2m}\right\}^{-1}. \qquad (5)$$

In this expression only m roots of the polynomial of the denominator are retained in z^{-1} which exceed the unit circumference (in terms of analog theory this means that the roots of the denominator of the transfer function $W(s)$ which lie to the left of the half-plane s (7) are retained). For the actual filter produced in study (9) with m = 5 and a cutoff frequency $\omega_c = 0.02\ c^{-1}$,

$$W(z) = \frac{10^{-15}(1 + 5z^{-1} + 10z^{-2} + 10z^{-3} + 5z^{-4} + z^{-5})}{1{,}00324 - 5{,}00972z^{-1} + 10{,}00972z^{-2} +}$$

$$\frac{}{+ 9{,}99020z^{-3} + 4{,}99029z^{-4} - 0{,}99070z^{-5}}. \qquad (5')$$

From expressions (5) and (5') it is evident that the structure of the filter turns out to be rather complicated. In a general case, 2m cells for storing the factors is required and during adjustment of the filter all the factors are varied. A high level of accuracy in representing the factors is necessary when designing a high order digital filter in linear mode. In addition, serious problems arise in the stability of the digital filter.

Similar high order filters may be implemented in general-purpose computers. In a specialized unit it is desireable to use a simpler and more conveniently implemented filter.

The structure and parameters of the Battervort filter considered previously are shown in study (9) and based on the spectral density values of the signal and noise. In order to determine the permissible limits of the filter characteristics, it is necessary to vary the criterion somewhat; specifically, it is predetermined by the required values of the transfer function in the area of the useful signal and the noise. The desired filter should produce a small attenuation of the signal and a practically complete quenching of the noise. An optimum filter in this case will serve as a reference, as a theoretical limit in accuracy.

Considering that the cutoff frequency of the signal during marine observations is approximately 0.003 Hz, the attenuation previously produced by the optimum filter, that is 3 dB, must be attained at this frequency. At the base frequency of oscillation of the ship (about 0.1 Hz) the attenuation should be at least 120 dB. Such noise from long-period oscillation of the sea level (1-2 min) which reaches 10-20 milligal is critical. Consequently, the attenuation at these frequencies should be at least 40 dB. From the large number of filters which achieve the assigned attenuation value, let us pick out those which have the highest-speed response and small phase distortions in the area of the useful signal along with an uncomplicated structure.

Transfer functions of the large category of filters which includes, in particular, the Battervort, Bessel', Chebyshev and other filters may be represented in the form

$$W(s) = \prod_{i=1}^{m} \frac{s_i}{s + s_i}. \qquad (6)$$

In the case which interests us, the terminals $-s_j$ are close to the virtual axis on the plane s. Here it approximates (2)

$$W(z) \approx \prod_{j=1}^{m} \frac{s_j T}{\left(1 - e^{-s_j T} z^{-1}\right)}. \qquad (7)$$

Thus it is logical to design the filter for the specialized digital computer unit STsVU in the form of a series connection of first order sections. A series structure for the filter is preferable also from the point of view of stability. A maximum high-speed response is achieved with $s_1 = s_2 = \ldots, s_m = a$ and consequently the desired filter will consist of identical sections.

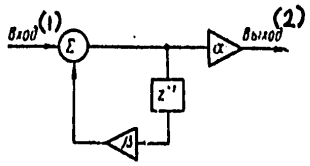

Fig. 1. Diagram of a First Order Recursive Filter

Key:
1. Input
2. Output

The transfer function

$$W(z) = \frac{aT}{1 - e^{-aT} z^{-1}} \qquad (8)$$

is a z-transform of the weighting function of the aperiodic section $W(t) = e^{-at}$.

With a sufficiently small interval of discreteness T and cutoff frequency a, the transfer function

$$W(z) = \frac{\alpha}{1 - (1-\alpha) z^{-1}} \qquad (8')$$

describes the simplest recursive filter schematically illustrated in figure 1. As shown in (3), such a filter is extremely easily implemented, especially when $a = 2^{-q}$. The simplicity of implementation makes it possible to carry out multistage filtering by formula (7).

Let us consider some of the characteristics of this filter. With the input signal x(nT) acting on the digital filter, the output signal is

$$y(nT) = \alpha \sum_{i=0}^{n} (1-\alpha)^i x(nT - iT). \qquad (9)$$

If x(nT) = 1 at the input, then we obtain the transient function $y(nT) = 1-(1-a)^{n+1}$. The frequency characteristic of the filter is determined by input to it of a discrete analog of the sine wave $x(nT) = e^{jn\omega T}$:

$$y(nT) = (1-\alpha)\, y(nT - T)\, e^{-j\omega T} + \alpha x(nT) = \frac{\alpha e^{jn\omega T}}{1 - (1-\alpha) e^{-j\omega T}},$$
$$y(nT) = |W| e^{j\Phi} x(nT), \qquad (10)$$

where

$$|W| = \alpha[1 + (1-\alpha)^2 - 2(1-\alpha)\cos\omega T]^{-1/2},$$

$$\varphi = \omega T - \operatorname{arctg}\frac{(1-\alpha)\sin\omega T}{1-(1-\alpha)\cos\omega T}$$

The periodicity of the frequency is apparent from (10). For a single-valued representation of a signal with discrete readouts, its maximum frequency ω must be less than π/T. If $\omega T \ll 1$, then the characteristics of (10) correspond to an analog system such as an RC filter with a time constant $\tau = T/a$.

During multistage filtering the requirements for sufficient attenuation with a noise frequency of 0.1 Hz will be met practically always and noise with 1-2 min periods will be more critical. In order to achieve attenuation of 40 dB at the frequency $\omega = 0.1c^{-1}$, the following time constants are needed for each section depending on the filter frequency:

m	4	6	8	10
τ	32	20	15	12,5
$\lvert W(f_0)\rvert$	0,7	0,82	0,86	0,88

The transfer constants in the frequency of the useful signal $f_0 = 0.003$ Hz are placed on the bottom row. It is apparent that the distortion of the useful signal with the indicated parameter combinations does not exceed acceptable limits.

The calculations shown indicate that the time constant of the filter and its frequency may be varied in rather broad limits depending on the problem at hand. As a result of this, the following section time constants are included in the described STsVU: 6.4, 12.8, 25.6 and 51.2 sec, with the smallest time constant intended for laboratory and test unit research and the largest for potential extremely unfavorable conditions. The filtering frequency may be adjusted up to m = 10.

Turning to the phase characteristics of this filter, a general observation must be made. It is known that the characteristics of the filter are improved considerably by inserting a time delay equal to $W^{-1}(s)$ when $s = 0$. In gravimetric surveying, a time delay is perfectly acceptable. Calculating the time delay during filtering with variable cutoff, for instance, means that the result of averaging is related to the mean of the cutoff. When filtering with an RC filter section it is necessary to include a time delay equal to the time constant.

If the phase characteristics turn out to be ideal when filtering with a variable cutoff or other filters with a symmetrical weighting function, phase distortions are inevitable for a filter with a transfer function (S). Nonetheless, with a large m the transfer function approximates the function of a section with the proper time delay and the phase characteristics are improved. This is illustrated in figure 2 in which phase characteristics are shown which allow for a shift in $m\tau$ for the following filters providing identical attenuation in frequency $\omega = 0.1c^{-1}$.

Since the phase distortions may be computed to be negligibly small only for a signal with a period greater than 1000 sec for two-stage filtering, a tenth order filter does not produce appreciable phase distortions up to a signal with a period of 100 sec.

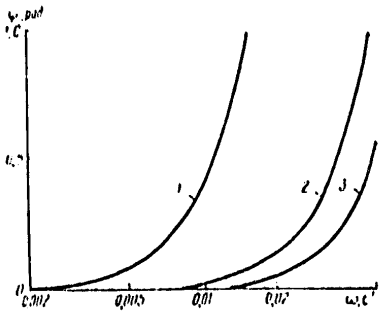

Fig. 2. Phase Characteristics of Filters

1— τ = 100 sec, m = 2; 2— τ = 20 sec, m = 6; 3— τ = 12 sec, m = 10.

Thus, the examined filter consisting of series connected numerical analogs of an aperiodic section achieves a small attenuation and insignificant phase distortions in the area of the useful signal and practically complete quenching of the noise. With the inclusion of a time delay, the filter has an order of astatism equal to two, that is upon completion of the transfer processes, the linearly varying useful signal is reproduced precisely (7). The described STsVU (fig. 3), like any digital computer, includes a data input unit (UVD), a unit for output of results (UVR), an arithmetic unit (AU), a main memory (OZU), a read-only memory (PZU) and a control unit (UU).

The input unit is for converting input values to a form convenient for computing. In this case the input unit of the STsVU is a converter of physical values to digital code. The conversion of signals of such parameters as those of TsAG's and taut-wire accelerometers are implemented by a frequency meter similar to that described in (6). A distinguishing feature is the availability of a binary counter in addition to the decimal counter. The

decimal counter is used for direct measurements, the binary for convenience in carrying out computing in the STsVU. The solutions given by such computing are more economical than using a decimal-binary converter. An interval of measurements is selected equal to 0.1 sec.

The output unit is for converting the results of computing to a form convenient for their further use and their output from the STsVU. Three forms of output data are included: recording the results of measurements with a discreteness of 0.1 sec on a tape recorder, punching the computing results at 10 and 60 sec intervals and converting the results to analog form and recording them on an automatic recorder.

The arithmetic unit is composed of two parts: a computing block for a sudden increase in gravitational force and a filtering block. Computing a sudden increase is done by formula (1). The difference $n - n_0$ is produced by setting the binary counter initially to the n_0 position with this value expressed in complement form. Thus, if Δn is positive it is represented in linear form; if negative it is represented in complement form.

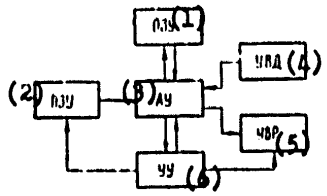

Fig. 3. Block Diagram of an STsVU

Key:
1. Main memory
2. Read-only memory
3. Arithmetic unit
4. Data input unit
5. Unit for output of results
6. Control unit

The codes k_1, k_2,--n_0 are set up in binary form by special switches.

All arithmetic operations are performed by serial codes which simplifies the unit design and makes it possible to improve the structure's flexibility and the modular design of the digital circuits. The adopted representation of numbers in complement form corresponds best to implementing the digital unit with serial arithmetic, since addition operations may be carried out beginning with low-order digits without previous knowledge of the numbers and without later correction of the sums obtained as in the case of reverse code.

The serial input accumulator for adding numbers in complement form is extremely simple in design. It consists of a complete binary adder with a delay in one digit for transferring a carry to the input.

For achieving a high level of accuracy of computing, multiplication is done by retaining all the digits of the product. This is possible because the

values of the operands are not independent due to the use of the calculation in the frequency meter without the loss of the counter pulses.

The filter is implemented in the previously considered cells (see fig. 1). Computing is done by a recursive formula resulting from the transfer function (8),

$$y(nT+T)=y(nT)-\alpha y(nT)+\alpha x(nT+T). \qquad (11)$$

Here, the filter version presented in (3) is used in which multiplication to the factor $a = 2^{-q}$ is replaced by a shift to q digits which simplifies the filter circuit considerably. Formula (11) using serial arithmetic makes it possible to construct a filter with only one register in contrast to the circuit shown in (3).

The STsVU memory is not isolated structurally in the form of a separate unit. The factors k_1, k_2 and n_0 are stored in the read-only memory. The main memory is allocated and composed of registers in the computer and filter.

The control unit produces the control signals needed for computing. A clock frequency of 10 Hz is preset by a crystal oscillator and the frequency dividers of the input unit.

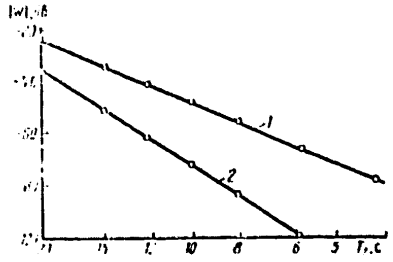

Fig. 4. Frequency Characteristics of the STsVU Filter

1-- m = 4; 2-- m = 6.

The STsVU is constructed of integrated microcircuits. Indeed, their use has made it possible to develop an effective instrument of this sort. The frequency characteristics of the STsVU, the transient and weighting functions have been plotted during laboratory research. Although the performance of the filter is described completely by any of these characteristics, it is more graphic to use all three for analyzing the corresponding frequency, time and phase characteristics of the system.

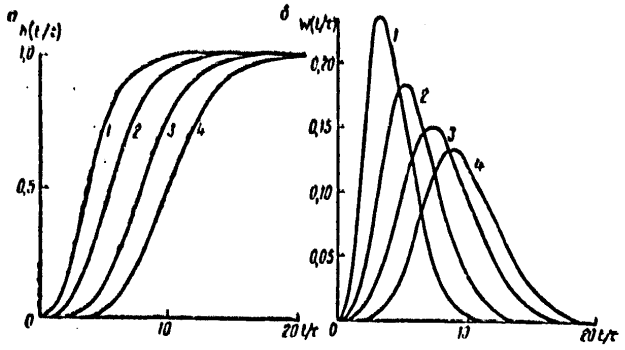

Fig. 5. Transient (a) and Weighting (b) Functions of the Filter

1-- m = 4; 2-- m = 6; 3-- m = 8; 4-- m = 10.

The frequency characteristic of the STsVU is plotted in the area of noise with the period Tz for the time constant $\tau = 6.4$ sec and m = 4 and 6 (fig.4). For large time constants and rates of acceleration it is impossible to analyze experimentally the value of the noise at the output of the filter. The plotted characteristics coincide with the theoretical, which attests to the accurate operation of the filter's digital circuits.

Although the characteristics of digital filters are calculated with a high level of precision, nonetheless it is interesting to study the system of gravimeters: filters for signals which simulate a gravitational field up to periods of 1000-2000 sec with an amplitude to several milligals.

Transient processes in the examined STsVU (fig. 5) may be characterized by the following values: the duration of the transient process, that is the time from the moment of input of the signal 1(t) to the moment when the signal reaches the value 0.99 at the output, the time delay from the moment of reaching the 0.5 level and the time for the gain to equal $1/y(t)_{max}$.

The dependence of these characteristics on the filter frequency (fig. 6) for the time of the transient process and the delay time with $m>4$ is practically linear, while the delay time is equal to $m\tau$. The delay time with large frequencies depends on m slightly. The weighting functions plotted experimentally (fig. 5) coincide with the theoretical as defined by the formula

$$W(t) = \frac{e^{-t/\tau} t^{m-1}}{(m-1)!\,\tau^{m-1}}.$$

Note that with an increase in the filtering frequency the weighting function becomes ever more symmetrical which corresponds to the conclusion on the improvement of the phase characteristics.

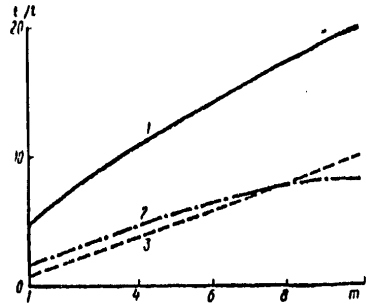

Fig. 6. Characteristics of Transient Processes

1--time of the transient process, 2-- delay time, 3-- increment time.

The stated theoretical and experimental data allows the following conclusions to be drawn.

1. The described STsVU has made it possible to record both a digital and an analog form of the value of gravitational force, filtered out from noise related to vertical accelerations by means of the operation of high-speed response gravimeters.

2. The use of an STsVU makes it possible for an operator to analyze the gravimeter operation and the nature of the gravitational field right at the time of the observations and to correct the filtering parameters depending on the conditions of the observations.

BIBLIOGRAPHY

1. Veselov, K. E.; and Gusev, G. S. "A New Digital Automated Gravimeter TsAG of the All-Union Scientific Research Institute of Geophysics," PRIKLADNAYA GEOFIZIKA, Issue 66, Moscow, Nedra, 1972.

2. Gold, B.; and Reyder, C. "Digital Signal Processing," Moscow, SOVETSKOYE RADIO, 1973.

3. Gornets, N. N.; and Staklo, A. B. "Methods of Linear Filtering for Digital Gravimeters," Moscow, Izd. VINITI, No 1844-70, 1970.

4. Lozinskaya, A. M.; Fomina, Z. I.; and Yashchayev, I. L. "Aerogravimetric Device based on Taut-wire Detectors," PRIKLADNAYA GEOFIZIKA, Issue 70, Moscow, Nedra, 1973.

5. Bobrov, Yu. V.; Gaynanov, A. T.; Gladun, V. A. and others. "Opredeleniye sily tyazhesti na more" [Determining the Gravitational Force in the Ocean], Moscow, Nedra, 1970.

6. Ivankin, L. G.; Simakov, V. S.; Staklo, A. V. and others. "An Experiment in Detained Gravimetric Surveying by Taut-wire Gravimeters in the Black Sea," IZV. AN SSSR SER. FIZIKA ZEMLI, No 9, 1974.

7. Pugachev, V. S. (ed.) "Osnovy avtomaticheskogo upravleniya" [Bases of Automatic Control], Moscow, Nauka, 1967.

8. Panteleyev, V. L.; Zhivitskaya, I. N.; and Ismalkhodzhaev, S. K. "Analysis of the Statistical Characteristics of an Agitation Accelerometer," MORSKIY GRAVIMETRICHESKIYE ISSLEDOVANIYA, Issue 4, Moscow, Izd. MGU, 1969.

9. Staklo, A. V.; Simakov, V. S.; and Kossova, K. A. "Gravitational Signal, Noise and a Survey of the Filtering Method using Gravimetric Measurement in the Ocean," Moscow, Izd. VINITI, No 157-74, 1974.

10. Tulin, V. A.; and Osinskaya, S. V. "Marine Gravimeter with Automated Readout," in "Apparatura i metody izmereniya sily tyazhesti na more" [Equipment and Methods for Measuring Gravitational Force in the Ocean], Moscow, Nauka, 1970.

11. "Tsifrovaya obrabotka signalov" [Digital Signal Processing], Moscow, MIR, 1975.

8945
CSO: 8144/0854B

GEOPHYSICS, ASTRONOMY AND SPACE

UDC 532.42

FIRST RESULTS OF SCIENTIFIC EXPERIMENTS ON 'VENERA-11' AND 'VENERA-12'

Moscow PIS'MA V ASTRONOMICHESKIY ZHURNAL in Russian Vol 5, No 1,1979 pp 3-7

[Text] Soviet interplanetary automatic stations "Venera-11" and "Venera-12." V. L. Barsukov, V. G. Zolotukhin, V. M. Kovtunenko, and R. Z. Sagdeyev. Soviet interplanetary automatic stations "Venera-11" and "Venera-12" are close in design to "Venera-10," however they were equipped with completely different instruments. The experiments conducted during the descent of the stations into the Venutian atmosphere were aimed at studying three main problems:

a) Fine chemical analysis of atmospheric gases;
b) Nature of clouds;
c) Thermal balance of atmosphere.

Below is a list of the instruments designed to study the atmosphere, and the problems for which the information obtained with their help is important are noted in parentheses:

1. Mass-spectrometer (a, b).
2. Gas chromatograph (a, b).
3. Optic spectrometer and photometer (a, b, c).
4. Nephelometer (b).
5. X-ray fluorescent spectrometer (b).
6. Instrument to measure electrical activity of atmosphere (b, c).

In addition measurements were made of temperature, pressure and aerodynamic G-forces. All the experiments were successful. Below are the first reports of their results. The dates of launching, landing, coordinates of the landing points, zenith distance of the sun at points of landing, as well as the pressure and temperature at the surface are as follows:

	"Venera-11"	"Venera-12"
Date of launching	9 October, 1978	14 October, 1978
Date of landing	25 December, 1978	21 December, 1978
Latitude	-13°	-7°
Longitude	300°	294°
Zenith distance of sun	19°	24°
Temperature on surface	735K	743K
Pressure on surface	92 atm	90 atm

The flight apparatus of the interplanetary automatic stations "Venera-11" and "Venera-12" after separation of the descent vehicle passed the planet at an altitude of about 34,000 km. They provided retransmission of information from the descent vehicle, and also carried a set of scientific instruments designed to study the upper atmosphere of Venus (UV-spectrometer, see below the report on the results), solar wind, cosmic sources of gamma-radiation. In the process of preparing and testing the set of scientific apparatus a system was set up for express processing of scientific information that made it possible to rapidly process data from the flight and descent vehicle.

Measurements of chemical and isotope composition of atmosphere with a mass-spectrometer. V. G. Istomin, K. V. Grechnev, V. A. Kochnev, V. A. Pavlenko, L. N. Ozerov, and V. G. Klimovitskiy. On the descent vehicle of "Venera-11" and "Venera-12" mass-spectrometric measurements were made on the atmospheric composition. In both experiments mass-spectrometers were engaged at altitude $\sim$24 km, and operated all the way to landing of the apparatus. A comparison of the mass-spectra from the two apparatus shows the complete identity of the findings. The main characteristics of the employed mass-spectrometers are such that the range from 11 to 105 MU is scanned in 7 s, whereby the resolution at level 0.1 peak is $\sim$35; the time for taking a gas sample is less than 5×10^{-3} s, frequency of sampling--once in 3 minutes. A total of 22 samples were taken and about 200 mass-spectra were transmitted to earth.

As a result of the measurements it was established that in addition to the main component--CO_2 the Venutian atmosphere has a considerable quantity of nitrogen (about 5 vol%). The mass-spectrometer also detected (as a small component) water vapor (a surplus at peaks 17 and 18 MU); there are indications of the presence of chlorine in comparable amounts (at 35 MU), sulfur (excess at peak 32 MU), and possibly, compounds containing chlorine and sulfur.

The isotope composition of carbon measured from ratios of peaks 13 and 12 MU, with error about 10% correspond to Earth's ($^{13}C/^{12}C \approx 1.1 \times 10^{-2}$).

The mass-spectrometer also recorded argon isotopes (36, 38 and 40 MU), neon (20 MU) and krypton (84 MU). The summary content of all the argon isotopes--about 10^{-2}0/0, content of neon -20--about 10^{-3}0/0, and krypton-84--5×10^{-4}0/0.

The isotope composition of argon in the Venutian atmosphere reveals a strong anomaly in comparison to the isotope composition of argon in the Earth's atmosphere: an abundance of "secondary" (radiogenic) isotope ^{40}Ar in the atmosphere of Venus equal to the summary abundance of "primary" isotopes of ^{36}Ar, ^{38}Ar. Relatively the abundances of both "primary" isotopes of argon in the Venutian atmosphere, on the other hand, agree well with those for the argon isotopes of Earth's atmosphere ($^{36}Ar/^{38}Ar \approx 5$).

Analysis of chemical composition of Venutian atmosphere by gas-chromatographic method. B. G. Gel'man, V. G. Zolotukhin, V. V. Kazakov, N. I. Lamonov, A. I. Lipatov, B. V. Levchuk, L. M. Mukhin, D. F. Nenarokov, B. P. Okhotnikov, A. V. Sinel'nikov, V. A. Rotin, and V. N. Khokhlov. The small-sized gas chromatograph "Sigma" was installed aboard the Soviet automatic stations "Venera-11" and "Venera-12" for chemical analysis of the Venutian atmosphere.

The main feature of the given chromatograph--use of a special ionization detector in which the admixture to be analyzed is ionized by metastable atoms of neon. In the beginning of the measuring cycle the chromatograph conducted a "dummy" analysis, verified its efficiency with the help of an electrical test-signal, and carried out calibration with the help of a control gas mixture. A special device for taking in the samples excluded the entrance into the instrument of foreign admixtures associated with the functioning of the releasable apparatus.

With the help of the gas chromatograph "Sigma" nine analyses were made of samples of the Venutian atmosphere. Express processing of the findings showed the presence in the atmosphere besides CO_2 (main component) of a whole number of gases--nitrogen (~2%), argon (~0.4 x 10^{-2}%), and carbon monoxide (several thousands of a percent). Based on the analyses made one can draw a preliminary conclusion about the presence in the Venutian atmosphere of sulfur compounds (including SO_2 on the level 10^{-2} volumetric percents).

Spectrophotometric study of scattering and absorption of solar radiation in the Venutian atmosphere. Yu. M. Golovin, V. I. Moroz, B. Ye. Moshkin, N. A. Parfent'yev, N. F. San'ko, and A. P. Ekonomov. On the descent vehicle after opening of the parachute every 10 s with the help of an instrument especially created for this purpose the spectrum of the diurnal Venutian sky was recorded in the range from 4,500 to 12,000 Å, and the angular distribution of brightness of scattered radiation for filters: 4,900, 7,100, 10,200, and 13,000 Å (effective wavelengths). The spectral channel of the instrument provides resolution of $\lambda/\Delta\lambda \approx 30$, photometric $\lambda/\Delta\lambda \approx 4$, with angular resolution of both channels about 15°. Study of the spectra of the Venutian diurnal sky on the Soviet releasable apparatus was carried out for the first time, on "Pioner-Venus" this task was not set up.

The findings (about 500 spectra and angular scans) demonstrated a gradual change in the distribution of energy in the spectrum for scattered solar radiation as the spacecrafts entered deeper into the atmosphere. This change was governed by aerosol scattering (on particles of clouds), gas Rayleigh scattering and absorption in absorption bands belonging to CO_2 and H_2O. In the spectra obtained directly from the surface and near it deep bands of CO_2 are visible (λ7,800, 8,700, 10,500 Å) and H_2O (λ8,200, 9,500, 11,400 Å). A broad region of true absorption, as yet unidentified, is observed at these altitudes in the interval 4,600-5,500 Å. In the interval from 6,000 to 8,500 Å the intensity of scattered solar radiation from the height of parachute opening to the surface is reduced roughly 10-fold; within the cloud layer--only 2-fold. The lower border of clouds is located at altitude about 48-50 km, and near it the volumetric scattering coefficient is the maximum.

As a result of an analysis and interpretation of this material it is proposed that data will be obtained on the chemical composition, structure of the cloud layer and thermal balance of the atmosphere.

Studies of aerosol component of the Venutian atmosphere. M. Ya. Marov, V. N. Lebedev, V. Ye. Lystsev, and K. K. Manuylov. The back-scattering nephelometer

installed on the descent vehicle is a source of modulated frequency for kHz of sounding radiation at wavelength 0.92 m with half width 0.015 m for the level 0.5, and photometer recording this radiation scattered by the external medium into the rear hemisphere in the range of angles 174-180° that are united into a single block.

According to the results of a preliminary analysis of the obtained information the conclusion was confirmed that was made on the basis of nephelometric measurements on "Venera-9" and "Venera-10" on the position of the lower border of clouds at altitude about 48-49 km. The cloud cover near the lower border (between 48 and 51 km) either possesses increased optic density, or here large particles with high refraction index n begin to make a noticeable contribution. Below the clouds the atmosphere as a whole is fairly transparent, however there are regions where due to the presence of aerosol the amount of back scattering increases. Besides the areas of aerosol that we previously noted near 14-17 km one can isolate a similar region between 5 and 10 km.

Based on the model that we proposed (large aerosol particles with small $\dot{r}_{ср} \geq$ 2.5μm, n≈1.8-2.0 and small volumetric concentration N≈1-2 cm^{-3}) one can hypothesize that the aerosol under the clouds, like the aerosol near the lower border of clouds is particles of sulfur (n=1.9), which agrees with Young's theoretical model. At the same time with regard for the effectiveness of exhalation of volatile substances with a high surface temperature and the probability of their condensation in the atmosphere at different levels it is impossible to exclude the possibility of another identification of the detected local regions of aerosol in the lower atmosphere of the planet.

Experiment "Groza." L. V. Ksanfomaliti, O. F. Ganpantserova, Ye. V. Petrova, and A. P. Suvorov. The task of the experiment was to study the electrical activity of Venutian atmosphere. A long-wave spectrum analyzer was used with range 8-100 kHz with an external antenna. It had an acoustic channel with external sensor.

The electromagnetic fields of an impulse nature found during the descent of "Venera-12" had degree of intensity 100-250 μV/m at 10 kHz and 20-30 μV/m at 18 kHz. The impulses were grouped into two separate packages and were lacking between them. At altitudes below 2 km and on the surface the amplitude of the impulses was very low.

A comparison of the results obtained by the two apparatus that had similar routes showed that the phenomena associated with the movement and electrification of the apparatus were insignificant. Only one group approximately made of 10^3 impulses at altitudes 5-11 km coincide. In the middle of the descent of "Venera-11" for 13 minutes a large group of impulses was recorded (up to 25 imp/s) with field intensity up to 700, 130, 40 and 6 μV/m at frequencies 10, 18, 36 and 80 kHz respectively. The falling spectral characteristics makes it possible, upon analogy with Earth's storms, to consider the source fairly distant. Another group of impulses apparently belongs to a source with small angular dimensions.

Thus a preliminary analysis of the experimental results makes it possible to hypothesize that the recorded impulses of the field are linked to processes

in the Venutian atmosphere. The frequency of succession of impulses greatly exceeds that observed during Earth's storms. Below the level 2 km and on the surface of the planet the field intensity drops sharply; it is not excluded that the lower layer of the Venutian atmosphere has a strong screening effect in the range 8-100 kHz.

The acoustic channel during descent of the apparatus recorded an aerodynamic noise with level over 88 db. During landing the noise ceased, after which there were individual impulse sounds linked to the operation of the apparatus. In 32 minutes after landing of "Venera-11" a sound was noted with level about 82 db of an unknown origin.

Study of scattered ultraviolet radiation in the upper Venutian atmosphere from the flight apparatus. Zh. L. Berto, Zh. E. Blamon, V. G. Kurt, A. S. Smirnov, and N. N. Romanova. To study the scattered ultraviolet radiation in the upper Venutian atmosphere a multiple-channel diffraction spectrometer to record simultaneously radiation in 10 spectral channels in the region of the spectrum from 300 to 1,657 Å was installed on the flight apparatus. The optic axis of the spectrometer was oriented roughly in an antisolar direction and scanned the illuminated disc of the planet during the near-planet session of measurements lasting over 2 h. The apparatus passed a distance 40,000 km (6.6 radii from the center of the planet), and the angular diameter of the planet was 17°. The optic axis of the spectrometer scanned the Venutian disc almost along the diameter: the minimum distance from the center of the planet was 3.4 and 4.5° (for "Venera-12" and "Venera-11" respectively). At the end of the session the visual beam passed a distance 3 radii from the center of the planet.

In the channel λ1,216 Å (HI) the rise in the signal was noticeable throughout the entire session, in the channel λ584 Å (HeI) there was also a certain rise noted in the signal far from the planet. In the other channels the signal differed from the level of the background only during sighting of the planetary disc. The table presents the rates of counting (in un. imp/s) for the background and illuminated disc, as well as the ratio of these amounts.

λ, Å	(1) $n_{фона}$	(2) $n_{диска}$	(3) $n_д/n_ф$	λ, Å	(1) $n_{фона}$	(2) $n_{диска}$	(3) $n_д/n_ф$
304	0.50	6.5	10.8	1216	28.4	1000	40
584	2.60	150	57.7	1300	2.08	80	38.4
736	3.6	11	3.05	1500	2.05	5.2	2.53
836	4.3	21	4.88	1657	2.32	3.7	1.59
1048	10.8	20	1.85				

Key:
1. $n_{background}$ 2. n_{disc} 3. n_d/n_b

In order to determine the intensity in the selected lines of the spectrum it is necessary to consider the scattered light in the spectrometer that mainly emerges from the radiation lines λ1,216 and 1,300 Å. The maximum of instrument sensitivity is reached near 800 Å (about 1 imp/s for 1 Rayleigh), on line λ1,216 Å the sensitivity drops to 1 imp/s for 10 Rayleighs.

The measurement data obtained from the two stations are in good agreement with each other.

Study of aerosol of the Venutian cloud layer. Yu. A. Surkov, F. F. Kirnozov, V. K. Khristianov, V. I. Gur'yanov, V. N. Glazov, B. N. Korchuganov, and A. G. Dunchenko. On the automatic interplanetary station "Venera-12" for the first time an attempt was made to determine the element composition of aerosol in the Venutian cloud layer with the help of an x-ray-flourescent analyzer.

The instrument consists of a detector block which was installed outside the hermetically sealed module of the descent vehicle, and multiple-channel analyzer of impulse amplitude placed within the hermetically sealed module. The detector block contains: a) Analytical section in which a filter for collecting aerosol, radioisotope sources and detectors of fluorescent radiation are located; b) Electronic section containing preamplifiers, and amplifiers, power sources and so forth; c) Microsupercharger to pump atmosphere through and settle aerosol on the filter. The multiple-channel analyzer of impulse amplitude has 256 channels with capacity of 2^{16} impulses in each channel. It is divided into 2 sections of 128 channels each in which signals enter from 2 detectors. The first records the spectrum of fluorescent radiation excited in the aerosol by the isotope source of iron-55, the second--by isotope source of cadmium-109.

The instrument operated on the segment of the parachute descent of the station in the Venutian atmosphere at altitudes approximately from 60 to 45 km above the surface. During the passage of this segment about 1 m^3 atmosphere was pumped through the instrument. Simultaneously with settling of the aerosol on the filter it was irradiated by radio-isotope sources and the spectra of the excited fluorescent radiation was recorded.

Measurements were made of 2 spectra in the ranges of energy from ~1 to 7.5 keV, and from ~1.5 to 15 keV, and a change was also recorded in the rate of counting during the accumulation of aerosol and measurement of spectra.

According to preliminary data the presence of chlorine was found in the composition of aerosol, and the presence of sulfur was not excluded while the presence of mercury in a quantity greater than 1×10^{-9} g/cm^3 was excluded.

Received 3 January, 1979

9035
CSO: 1870

PHYSICS

UDC 621.375.826.038.823

INVESTIGATING THE NOISE CHARACTERISTICS OF AN OPTICAL AMPLIFIER IN A XE-HE MIXTURE (λ = 3.51 microns)

Moscow RADIOTEKHNIKA I ELEKTRONIKA in Russian No 1, 1979
signed to press 12 Sep 77 pp 91-94

[Article by V. P. Logvinov, I. P. Mazan'ko and V. A. Tsar'kov]

[Text] The results of investigating the noise of a receiving system, consisting of a photodetector and sectional single-mode optical amplifier with high amplification factor (on the order of 10^7) are reported. It is shown that the noise introduced by the optical amplifier is technical in nature and the modulation noise is considerably less than the additive noise with input laser signal power less than 10^{-12} W. The photodetecting system in the frequency range from 10 to 100 kHz had a threshold sensitivity on the order of 10^{-16} W/Hz$^{1/2}$.

One of the most important characteristics of a weak signal optical amplifier (OU) is the noise introduced by it. The additive noise of OU spontaneous emission impinging on the photodetector and so-called multiplicative or modulation noise are distinguished. Estimates from the results of previous investigations show that natural additive noise of a xenon-helium amplifier of special design (optimum by noise) [1, 2] has a value on the order of 10^{-17} W/Hz$^{1/2}$, which is considerably less than threshold sensitivity of standard infrared photodetectors. However, available data on the noise characteristics of xenon-helium OU [3, 4] are usually

qualitative in nature and do not permit one to make specific conclusions either about the capabilities of these OU or about the nature of their natural noise. The results of investigating the noise of a xenon-helium OU, which has a high amplification factor (K approximately $5 \cdot 10^6$) are outlined in this paper.

The investigations were conducted on an installation whose diagram is presented in Figure 1. The emission of xenon-helium laser (optical generator OG) operating at a wavelength of 3.51 microns, passed through a glass attenuator O, matching lenses L_1 and L_2 and entered the optical amplifier OU. The amplified emission was detected by a photodetector FP, as which a photoresistor, cooled to nitrogen temperature, based on indium antimonide with threshold sensitivity of $6 \cdot 10^{-11}$ W/Hz$^{1/2}$ at a frequency of 100 kHz, was used. One of the mirrors of the probing OG was placed in piezoceramics PK, which made it possible to readjust its frequency; the output emission was modulated by a mechanical breaker P. The OU operated in a single diffraction mode [1] and consisted of two stages K_1 and K_2, matching between which was accomplished by a lens L_4 and diaphragms D_1 and D_2. Lenses L_3 and L_5 formed the input and output beams, respectively. The photoresponse voltage was amplified by a preamplifier PU and was fed to the spectral analyzer AS input.

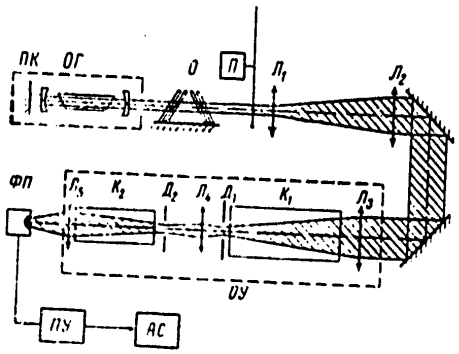

Figure 1. Diagram of Experimental Installation.

The spectra of the photodetector noise, caused by spontaneous emission of the OU and by the amplified laser signal, are shown in Figure 2, a. The spontaneous emissive power of the OU impinging on the photodetector had a value of approximately 5 μW, while the intensity fluctuations of the probing OG (with power of the last order of several microwatts) were negligible over the entire range of investigated frequencies. It is obvious that all the graphs have sharp rises in the region of 30-40 kHz and approximately 70 kHz, apparently caused by the presence of regular plasma oscillations (strata) in the discharge.

The spectrum of the discharge current fluctuations of the first stage K_1 is shown in Figure 2, b for comparison. It is easy to note the specific correlation between the spectra and Figure 2, a and b (for current of 21mA). We note that the spectra of spontaneous emission fluctuations and the spectra of current fluctuations of the second stage have no sharply marked rises at typical frequencies.

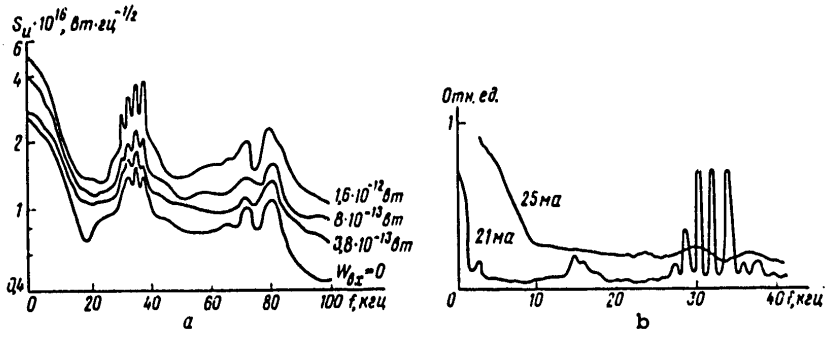

Figure 2. Spectra Reduced To OU Input Of Noise (a) And Discharge Current Fluctuations Of First Stage (b). The numbers near the curves indicate the input laser signal power W_{vkh} (a) and the value of the first stage discharge current (b). The second stage current is 10mA.

The shape of the spectrum and the absolute value of the spectral density of noise are strongly dependent on the first stage discharge current of the OU (Figures 2, b and 3). The dependence of the signal/noise ratio on the values of the discharge currents of the stages are shown in Figure 3. Reception was accomplished at a frequency of 1 kHz (the mechanical cut-off frequency of the OG signal) and the radio-amplifier band comprised approximately 60 Hz. Figure 3 shows that the maximum amplification is shifted to the range of high currents with respect to the maximum signal/noise, i.e., amplification is maximum in the region of a sharp increase of plasma fluctuations.

An increase of input laser signal power leads to an increase of amplifier noise due to modulation addition (Figures 1 and 4). Measurements at a frequency of 1 kHz showed that the modulation noise increases, as one would expect, in proportion to the input laser signal power (with variation from 10^{-14} to 10^{-11} W) and it is comparable in value to additive noise at power of approximately 10^{-12} W (Figure 4). The further increase of input signal power (from 10^{-11} to 10^{-9} W) did not lead to an increase of modulation noise due to amplifier saturation [5]. Moreover, the total amplifier noise level even decreased due to a decrease of additive noise, since the latter is the product of the spontaneous emissive power of the effective source located at the beginning of the OU by its amplification factor for spontaneous emission [5] (the latter was saturated by the laser signal). However, a drop of OU amplification occurs more rapidly than a decrease of noise since the saturated OU has worse noise characteristics compared to a linear (unsaturated) OU.

The results of the investigations permit one to make the following conclusions.

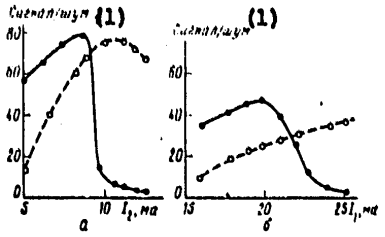

Figure 3. Dependence Of Signal/Noise Ratio On Discharge Current: a-of second stage (W_{vkh} = $2.0 \cdot 10^{-11}$W, the first stage is switched off) and b-of the first stage (W_{vkh} = $1.7 \cdot 10^{-13}$W, the second stage current is 8.5mA). The dependence of amplification on current (in relative units) is shown by the dashed line.

KEY:

1. Signal/noise.

1. The noise of a photodetector plus xenon-helium OU system was determined in the given case primarily by plasma parameter fluctuations. Local fluctuations (along the discharge length), which lead to relatively deep modulation of the intensity of the spontaneous emission source, apparently have the most significant effect on OU noise.

2. The spectral density of the additive noise of a xenon-helium OU with high amplification (on the order of 70 dB) comprises a value on the order of 10^{-9} W/Hz$^{1/2}$, which exceeds the threshold sensitivity of infrared photodetectors by more than an order.

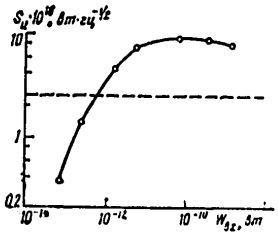

[Caption for Figure 4 on following page]

Figure 4. Modulation Noise Reduced To OU Input As A Function Of Input Laser Emissive Power W_{vkh}. The additive noise level is shown by the dashed line.

3. The shape of the spectrum and the absolute value of the spectral noise density of the OU are considerably dependent on the values of the discharge currents of the stages and the optimum signal/noise ratio does not coincide with the maximum amplification as a function of current.

4. Modulation noise is significantly less than additive noise at input laser signals with power less than approximately 10^{-12} W.

5. The linear operating mode of an OU is preferable since a nonlinear optical amplifier has considerably worse noise characteristics.

In conclusion the authors feel it their duty to express deep gratitude to Yu. V. Denisov for fruitful assistance in the paper and participation in discussion of the results.

BIBLIOGRAPHY

1. Logvinov, V. I. and V. A. Tsar'kov, KVANTOVAYA ELEKTRONIKA, Vol 3, 1976.

2. Logvinov, V.I. and V. A. Tsar'kov, KVANTOVAYA ELEKTRONIKA, Vol 3, 1976.

3. Kluver, J. W., J. APPL. PHYS., Vol 37, 1966.

4. Kuznetsov Ye. P. and I. P. Mazan'ko, ZH. PRIKL. SPEKTROSKOPII, Vol 7, 1967.

5. Mazan'ko, I. P. and M. V. Sviridov, OPTIKA I SPEKTROSKOPIYA, Vol 23, 1972.

6521
CSO:8144/0823

PHYSICS

UDC 621.375.826.038.823

INVESTIGATING THE NOISE OF A DC DISCHARGE PLASMA IN AN OPTICAL AMPLIFIER OPERATING IN A MIXTURE OF HE AND XE

Moscow RADIOTEKHNIKA I ELEKTRONIKA in Russian No 1, 1979 signed to press 12 Sep 77 pp 95-98

[Article by V. I. Logvinov, N. I. Reznichenko and V. A. Tsar'kov]

[Text] The results of investigating the noise of a DC discharge plasma in an opitcal amplifier operating in a HE-XE mixture are reported. It is shown that the DC discharge in a HE-XE mixture is characterized by the presence of a zone of reactive oscillations (at low currents), strata (at high currents) and an oscillation-free section (in the intermediate region of currents). The current boundaries of the oscillation-free section are constricted with an increase of filament voltage. When the strata are excited, they are amplified in the direction toward the cathode and the local percentage modulation of the lateral spontaneous emission in the visible region of the spectrum may reach 100 percent. The strata had the following characteristics: wavelength of approximately 1cm, frequency of approximately 30kHz and phase velocity of approximately 10^4cm/sec.

The optimum quantum noise level for two-stage design noise for xenon-helium opitcal amplifier (OU) (λ = 3.51 microns) is several orders below the noise level of the best infrared photodetectors [1]. However, it has been noted in the literature [2] that the additive noise of OU may have a value appreciably exceeding the sensitivity threshold of a standard

photodetector. This noise is apparently technical in nature and may specifically be caused by fluctuations of plasma parameters. We note that there is practically no data in the literature on investigation on the noise properties of a discharge in a xenon-helium mixture. The results of investigating the conditions for the occurrence and the existence of oscillations in a discharge plasma in the cuvettes of a xenon-helium OU are outlined in this paper.

The OU cuvette was placed on a movable platform which could be moved along the horizontal axis with respect to a vertical slit diaphragm. The lateral spontaneous emission of the narrow section of the discharge (on the order of 1mm) passed through the glass wall of the cuvette, was modulated by a mechanical breaker and was detected by a photodetector, as which a silicon photodiode with maximum sensitivity in the visible region of the spectrum was used. The photoresponse voltage was amplified by a radio preamplifier and was fed to a spectral analyzer and synschronous detector. The current fluctuation signal (which was a reference signal for synschronous detection when measuring the wavelength of the strata) was taken from the resistor in the cathode discharge circuit. The currents in both arms of the cuvette were balanced during measurement. The cuvette parameters used in the experiments are presented in the table. All the cuvettes had two-anode design with central hot cathode and were equipped with a bypass channel which made it possible to eliminate separation of the mixture due to cataphoresis.

№	(1) Внутренний диаметр, мм	(2) Длина разрядного промежутка, мм	(3) Соотношение парциальных давлений He:Xe	(4) Общее давление, тор	(5) Примечания
1	6	400	15:1	2,4	кольцевой(6) прессованный и штыревой аноды
2	10	310	30:1	1,7	кольцевые(7) прессованные аноды
3	6	400	15:1	4,8	

[Key for table on following page]

KEY:

1. Inner diameter, mm
2. Length of discharge interval, mm
3. Partial pressure ratio of HE:XE
4. Total pressure, torr
5. Comments
6. Annular molded and pin anodes
7. Annular molded anodes

We note that the necessity of operating in the visible region of the spectrum was caused by the absence of appropriate infrared photodetectors. The low threshold sensitivity of the latter makes it impossible to record lateral spontaneous emission at a wavelength of 3.51 microns. However, the nature of the behavior of spontaneous emission in the infrared and visible regions of the spectrum should not differ significantly since the xenon levels are populated primarily as a result of direct electron impact [3].

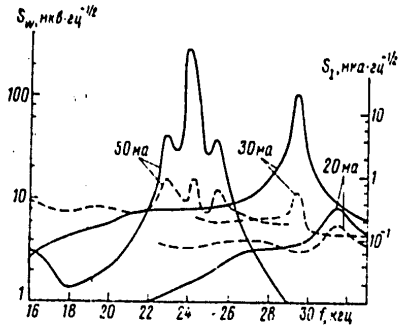

Figure 1. Emission (Solid Curves) And Current (Dashed Curve) Noise Spectra For Cuvette 1 With Filament Voltage Of U_n = 11V. The numbers near the curves indicate the value of the discharge current.

The intensity fluctuation spectra of lateral spontaneous emission S_W and of discharge current S_I for a cuvette 1 (see table) at different values of discharge current I_r (here and

further we have in mind current in each arm of the cuvette) are presented in Figure 1. The appreciable correlation between the spectra is clearly obvious; both have typical peaks which indicate the presence of regular oscillations. The spectral noise density increases with an increase of discharge current, the spectrum is enriched with new components and the frequency of the main oscillation decreases. The typical pattern of intensity modulation distribution of lateral spontaneous emission along the length of the cuvette (see Figure 3, a) permits one to assume that these regular oscillations are strata [4-6]. The similarity of the current fluctuation and emission intensity fluctuation spectra is explained by the fact that the traveling strata modulate the discharge current. Sharp peaks were detected at frequencies of 8-9 kHz and (considerably less in a value) at frequencies of 16-18 kHz, caused by the presence of reactive plasma oscillations [7], for this same cuvette at currents less than the lower boundary of existence of the strata. The amplitude of these peaks was approximately constant along the length of the cuvette, as was the difference of the signal and discharge current phases. Moreover, a drop of the percentage modulation of emission and discharge current with an increase of the latter was observed. The dependence of the frequencies of the strata and reactive oscillations on a discharge current are presented in Figure 2. One should note the presence of hysteresis and sections with positive slope for the stratal branch.

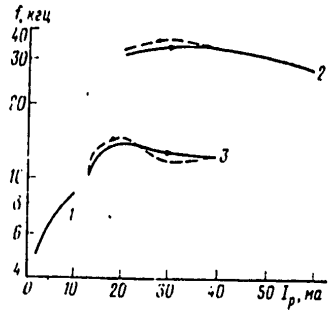

[Caption for Figure 2 on following page]

Figure 2. Dependence On Current: 1-reactive oscillation frequency in cuvette 1; 2-of strata in cuvette 1; 3-of strata in cuvette 2. The arrows on the curves indicate the direction of current variation.

The results of measuring the percentage modulation M of the lateral emission of cuvettes 1 and 2 by strata at different discharge currents are presented in Figure 3, a and b. It is obvious that amplification of the strata occurs toward the cathode (unlike a neon-helium mixture where the strata are amplified toward the anode [5]). We note that amplification of the strata toward the cathode is also observed in pure helium and xenon [8; 9]. The distribution of percentage modulation is symmetrical with respect to the cathode for cuvette 2. The asymmetry of distribution for cuvette 1 was apparently caused by the fact that, unlike cuvette 2, it had different anodes: an anode in the form of a molybdenum rod (the left anode in Figure 3, a) and an annular molded anode. The dips near the cathode on the curves of percentage modulation distribution may be caused by inhomogeneity of the cuvette channel near the cathode outlet and possibly by the mutual effect of strata in different arms. Typical fluctuations of the percentage modulation of emission along the cuvette axis are observed at currents slightly exceeding the threshold value of the occurrence of strata and modulation disappears near the cathode. These fluctuations are determined by interference between the members, one of which describes the distribution of strata along the cuvette axis and the other of which describes modulation of discharge current [10, 11]. We note that the distance between adjacent maximums is equal to the wavelength of the strata. The amplification index of the strata was determined by the slope of the linear section of the curves and had a value on the order of 0.1 cm^{-1}.

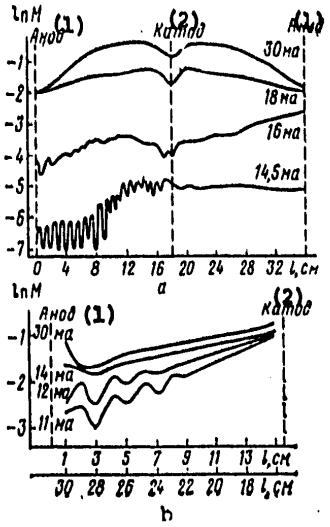

Figure 3. Distribution Of Percentage Modulation Of Lateral Discharge Emission Along the Length Of a Cuvette: a-for cuvette 1; b-for cuvette 2. The numbers near the curves indicate the value of the discharge current.

KEY:

1. Anode
2. Cathode

The strata were artifically excited to measure the dispersion characteristic and to estimate the value of the phase velocity, for which a voltage from an audio generator was fed to the anode circuit of a cuvette 3 (see Table) through a separating capacitor (with value of 150 pF). The derived function is easily approximated by the expression

$$f=1{,}3\cdot 10^{4}(1/\lambda_0-0{,}15)^{-1},$$

where f is frequency in hertz and λ_0 is the wavelength in centimeters. It is obvious that, as in the case of pure xenon [9], the phase velocity is negative. The phase velocity of a natural strata, determined by the slope of the curve $f(1/\lambda_0)$ at the corresponding point, was equal to $-1.8 \cdot 10^4$ cm/sec.

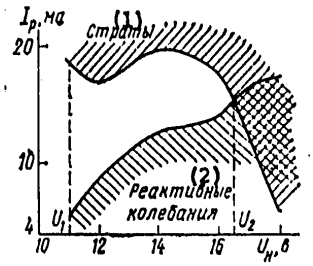

Figure 4. Dependence Of Current Boundaries Of The Existence Of Oscillations In A Discharge Plasma In Cuvette 1 On The Cathode Filament Voltage

KEY:

1. Strata
2. Reactive oscillations

The cathode filament voltage has a significant effect on the width of the current region in which there are no regular plasma oscillations. The boundaries of this region are shown in Figure 4 as a function of filament voltage. The maximum width of the region is achieved at the lowest voltage U_1, determined by the normal operating conditions of an oxide cathode. The current boundaries of the regions of existence of strata and reactive oscillations intersect at specific voltage U_2 and a region appears in which these oscillations may exist simultaneously. A characteristic feature is that the strata in this region are excited by the second harmonic of relaxation oscillations. We note that constriction of the region where there are no regular oscillations may be caused by the indicated synchronization since a reverse effect is observed in some cases; an increase of filament current leads to expansion of this region [7, 12].

The results of the investigations permit one to make the following conclusions.

1. A DC discharge in a xenon-helium mixture is characterized by the presence of three typical regions as a function of its value: regions of the existence of strata (at high currents), reactive oscillations (at low currents) and an oscillation-free region, while the boundaries of the latter are constricted with an increase of filament voltage.

2. The strata are amplified from the anode to the cathode and amplification is subject to exponential law with index of approximately 0.1 cm^{-1} in the initial section.

3. An increase of the total pressure of the gaseous mixture leads to a decrease of the typical frequency of the strata: from approximately 30 kHz at pressure of 2.4 torr to approximately 20 kHz at 4.8 torr.

4. The local (along the length of discharge) percentage modulation of lateral spontaneous emission by strata may reach 100 percent.

5. The shape of the anode affects the conditions for the occurrence and existence of strata at small values of discharge current (and, accordingly, at low amplification factors of the strata).

6. Phase velocity is opposite to group velocity in direction and has a value on the order of 10^4 cm/scc.

BIBLIOGRAPHY

1. Logvinov, V. I. and V. A. Tsar'kov, KVANTOVAYA ELEKTRONIKA, Vol 3, 1976.

2. Kuznetsov, Ye. P. and I. P. Mazan'ko, ZH. PRIKL. SPEKTROSKOPII, Vol 7, 1967.

3. Moskalenko, V. F. et al, OPTIKA I SPEKTROSKOPIYA, Vol 23, 1967.

4. Suzuki, T., JAPAN J. APPL. PHYS., Vol 9, 1970.

5. Basayev, A. B., M. I. Molchanov and N. G. Yaroshenko, ZHTF, Vol 45, 1975.

6. Burnashev, M. N., V. Ye. Privalov and Ya. A. Fofanov, OPTIKA I SPEKTROSKOPIYA, Vol 42, 1977.

7. Zakharenko, Yu. G. and V. Ye. Privalov, OPTIKA I SPEKTROSKOPIYA, Vol 35, 1973.

8. Ohe, K. and I. Takeda, JAPAN J. APPL. PHYS., Vol 11, 1972.

9. Yoshimoto, H. and Y. Yamashita, J. PHYS. SOC. JAPAN, Vol 22, 1967.

10. Nedospasov, A. V., USPEKHI FIZ. N., Vol 94, 1968.

11. Landa, P. S. and Yu. V. Ponomarev, RADIOTEKHNIKA I ELEKTRONIKA, Vol 21, No 11, 1976.

12. Vorob'yeva, I. A. et al, ZHTF, Vol 44, 1974.

6521
CSO:8144/0823

PHYSICS

UDC 621.375.826

CONTROLLING THE PARAMETERS OF MICROSECOND EMISSION PULSES

Moscow RADIOTEKHNIKA I ELEKTRONIKA in Russian No 1, 1979
signed to press 20 Dec 77 pp 105-108

[Article by V. V. Arsen'yev, I. N. Matveyev and A. N. Stepanov]

[Text] The results of experimental investigation of the effect of different laws of Q-switching on the shape, length, amplitude and stability of microsecond pulses of ruby laser emission with negative feedback are presented. It is shown that the possibilities of controlling the microsecond emission pulse parameters increase significantly when using a modulating pulse consisting of a jog corresponding to rapid Q-switching, a pulse peak slowly increasing by exponential law and a steep trailing edge. The instability of the moment of initial generation decreased to a value of approximately 25 nsec when using step connection of the cavity Q-factor.

One of the most effective methods of increasing the emission pulse length of solid-state lasers with Q-switching to microseconds or more is the use of negative feedback (OOS) and slow connection of cavity Q-factor [1-3]. It follows from analysis of balance equations of this laser that the shape of the emission pulse is considerably dependent on the law of cavity Q-switching [1]. It is very difficult to

derive theoretically the required law of Q-switching for different pulse shapes. In the simplest case, the cavity Q-factor should vary by exponential law to shape square-wave emission pulses, which provides equality of amplification and losses in the cavity [4]. The law of switching close to exponential was used in experimental investigations of lasers with OOS described in [1-3].

The results of investigating the effect of various laws of cavity Q-switching on the shape of the microsecond pulse of a RL-8X120/180 ruby laser with electrooptical feedback are presented in the given paper. The diagram of the experimental installation is similar to that described in [3]. The laser cavity 0.6m long had a configuration close to semiconcentric. A smoother emission pulse peak is achieved with this configuration [2]. The cavity Q-factor was controlled by a DKDP crystal light shutter, to whose electrodes modulating pulses and negative feedback voltage were fed. The modulating voltage pulses were shaped by a special generator which permits regulation of their parameters.

Generation of a laser with feedback having slow law of cavity Q-switching was initially investigated. The shape of the modulating voltage on the shutter electrodes (Figure 1, a) was approximated to the form

$$U_0 - U(t) = \frac{U_{\lambda/2}}{\pi} \arccos\left\{2K_0 \exp\left(-\frac{t}{\tau}\ln\frac{K_0}{\alpha(\tau)}\right) - 1\right\}, \quad (1)$$

where $U_{\lambda/2}$ is the half-wave voltage of the shutter, K_0 is the amplification factor, τ is the emission pulse length, $\alpha(\tau)$ are the losses in the cavity with completely open shutter and U_0 is the shutter cut-off voltage. Emission pulses 1-3 μsec long with flat peak and smoothly decreasing trailing edge were shaped in this case. The generated pulses had high instability of the moment of formation of the leading edge (Δt_n) with respect to initial connection of the modulating pulse (Δt_n 200 nscc). Analysis of the experimental data showed that this

instability has the greatest effect on the shape of emission pulses, since the value and steepness of the modulating voltage at which the leading edge of the pulse is formed vary in this case.

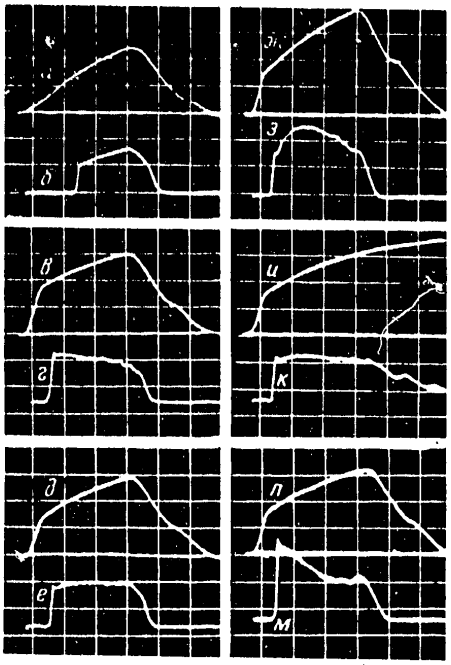

Figure 1. Control Of The Emission Pulse Shape.
The oscillograms of the control voltage pulses (upper pulses, calibration of 500 V/div) and the corresponding emission pulses (lower, calibration of 60 kW/div) at E_n = 610 J and K_{os} = $3.75 \cdot 10^{-3}$ V/W) K_{os} = $1.5 \cdot 10^{-3}$ V/W 4m). Scanning was 0.5 μsec/div

To stabilize the moment of the beginning of generation and also the shape of the emission pulse, it was suggested that complex cavity Q-switching be introduced (Figure 1, c). To do this, the modulating voltage pulse was a jog corresponding to fast cavity Q-switching which changed to a slowly increasing modulating pulse peak variable by law (1) and had a steep

trailing edge. The use of this modulating pulse made it possible to rigidly stabilize the moment of the beginning of generation of the emission pulse. The measurements showed that instability Δt_n decreased to a value of approximately 25 nsec with this law. At the same time, the stability of the emission pulse shape increased significantly. Variation of the square-wave pulse amplitude in the form of Figure 1, f from burst to burst did not exceed 5 percent over the entire length.

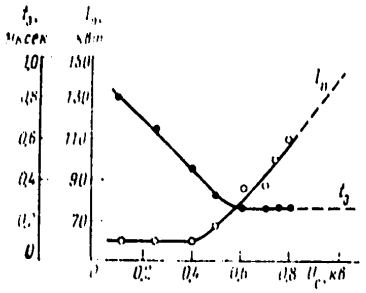

Figure 2. Dependence Of The Amplitude Of The Leading Edge Of The Emission Pulse On Value Of Jog U_s; E_n = 610 J and S = 0.5 kV/ μsec

An important positive feature of introducing a jog in the modulating pulse was to expand the possibility of controlling the shape of the emission pulse. The amplitude of the jog U_s affects the emission pulse delay t_z with respect to the leading edge of the modulating pulse and the amplitude of the leading edge of the emission pulse I_p. Oscillograms of emission pulses at different amplitudes of jog U_s are presented in Figure 1, d and f. The experimental dependence of I_p and t_z on U_s are presented in Figure 2. It follows from them that delay of the moment of the beginning of pulse generation t_z decreases with an increase of U_s, reaching some practically constant value determined by the time of development of generation. In this case the amplitude of the leading edge of the emission pulse I_p does not change initially, but then increases rapidly. This dependence of I_p on U_s permits one to tranform square-wave

emission pulses to triangular pulses with steep leading and extended trailing edges (Figure 1, d and o).

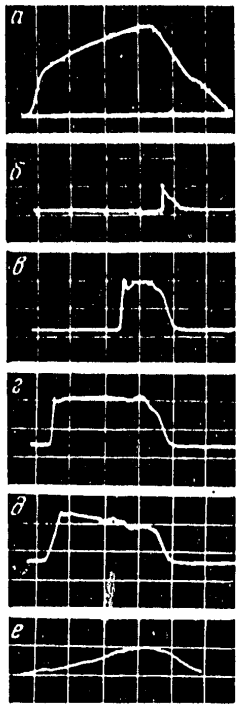

Figure 3. Variation Of Emission Pulse Shape With Increase Of Pumping Energy E_m: b - 190 J; c - 450 J; b - 610 J; e - 800 J; K_{os} = 3.75 V/W; a - oscillogram of modulating pulse corresponding to them; f - emission pulse with slow cavity Q-switching and at E_n = 800 J and $K_{os} = 6.25 \cdot 10^{-3}$ V/W

By cutting off the cavity Q-factor at the necessary moment of time, one can cut the descending trailing edge of the emission pulse (Figure 1, e, f, i and j) and one can shape pulses close to square-wave and one can also change their length.

Regulation of the emission pulse length is also possible by varying the pumping energy E_n. The delay of the beginning of generation t_z decreases and the emission pulse length increases with an increase of E_n. In this case the pulse amplitude varies slightly (Figure 3). The pulse shape changes to triangular (Figure 3, b) with pumping close to generation threshold. The segment of the modulating voltage pulse corresponding to slow cavity Q-switching determines the shape of the emission pulse peak. Square-wave emission pulses are formed during selection of the law of variation of the modulating voltage on this section which provides equality of amplification and losses (Figure 1, f). The slope of the emission pulse peak can be regulated and it can be made convex by changing the steepness S of this segment of the modulating pulse (Figure 1, h). The amplitude of pulse convexity I_v increases with an increase of steepness S (Figure 4). By changing the amplitude of the modulating pulse jog U_s and the steepness of the voltage increase at the modulating pulse peak S, one can find square-wave emission pulses with different amplitudes, which is not achieved when using modulating pulses without a jog. Regulation of the emission pulse amplitude is also possible by varying the depth of feedback (Figure 1, f and l). However, this method has limited use since a decrease of negative feedback increases the cut of the emission pulse peak and makes its overall stability worse.

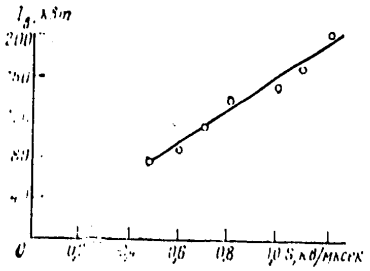

Figure 4. Dependence Of Pulse Convexity I_v On Modulating Pulse Steepness S; U_s = 0.7 kV and E_n = 610 J

By using slow switching law (Figure 1, a) with high value of pumping energy E_n and deep feedback ($K_{os} = 6.25 \cdot 10^{-3}$ V/V), pulses with steep leading edge may be transformed to pulses with smoothly increasing amplitude (Figure 3, f). This transformation of pulse shape is related to the fact that the generation threshold is carried out with high losses on the light shutter which provide a slow increase of the number of photons in the cavity.

Thus, the investigations showed that the use of special stepped modulating voltage pulses permits one to increase the stability of microsecond emission pulses and to expand the possibility of controlling their length, amplitude and shape.

BIBLIOGRAPHY

1. Balashov, I. F., V. A. Berenberg and B. A. Yermakov, ZHTF, Vol 43, No 7, 1973.

2. Arsen'yev, V. V., V. N. Lomakin, I. N. Matveyev and A. N. Stepanov, KVANTOVAYA ELEKTRONIKA, Vol 3, No 5, 1976.

3. Arsen'yev, V. V., I. N. Matveyev, Yu. V. Prichko and A. N. Stepanov, PRIBORY I TEKHNIKA EKSPERIMENTA, No 2, 1976.

4. Balashov, I. F., V. A. Berenberg and B. A. Yermakov, ZHTF, Vol 38, No 5, 1968.

6521
CSO:8144 /0823

PHYSICS

UDC 535.231.12.038.62:621.317.794

A METHOD OF RESTORING LASER BEAM ENERGY DISTRIBUTION FROM DATA OBTAINED FROM A BOLOMETRIC SENSOR ARRAY

Moscow RADIOTEKHNIKA I ELEKTRONIKA in Russian No 1, 1979, signed to press 24 Aug 77 pp 193-196

[Article by V. V. Yefremenko]

[Text] Existing methods of investigating the distribution of laser energy in the beam cross-section are usually related to the necessity of branching part of the energy to a measuring device [1], which is difficult to accomplish at high energy densities and large beam cross-sections. The use of an array of bolometric wire sensors in combination with a specific processing algorithm makes it possible to measure the energy distribution over a wide spectral range [2], having avoided the necessity of energy branching. A method of determining the energy center and effective beam diameter by using bolometers is described [3], but this method does not permit one to measure the energy distribution. At the same time an important advantage of reticular bolometric sensors, consisting in the fact that they do not introduce significant distortions in the transient laser beam, provides the basis to attempt to use them as an energy distribution meter.

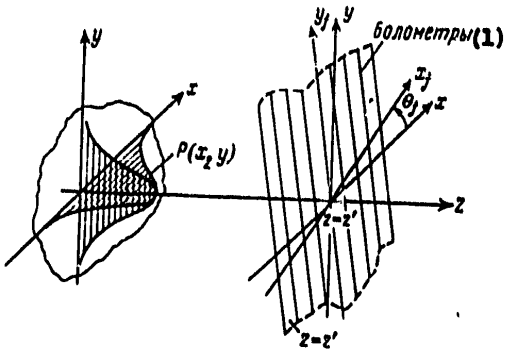

Figure 1. Arrangement Of Bolometer Array With Respect To Laser-Bound Coordinate System

KEY:

1. Bolometers

To simplify further consideration, let us make a number of assumptions. Let us assume the following:

(1) the spacing of the bolometric arrays h is much greater than the laser emission wavelength λ and the bolometer diameter d, i.e., we assume that the mutual effect of the bolometers during diffraction of the emission on the grid may be disregarded;

(2) the grid dimensions are much greater than the typical cross-sectional dimensions of the laser energy concentration zone and integration can be carried out within infinite intervals;

(3) laser emission has circular polarization;

(4) the laser pulse length τ_i is much less than the constant bolometer cooling time;

(5) the effect of emission does not lead to thermal expansion of the bolometers, while the dependence of bolometer resistance on emission intensity is linear.

Let laser emission be propagated along axis Oz in a coordinate system $\{x, y, z\}$, bound to a laser source (Figure 1). The value of power W (x, y, z, t) in plane z=z', located in the Frauenhofer zone, will be a cross-section of the space-time power distribution of the laser source at z=z'. Let us further assume that the axes of parallel wire bolometers with diameter d and spacing h are located in this same plane. Let us also assume that there are several arrays of parallel bolometers and that they are arranged rather close to each other along axis Oz. Let us describe the orientation of the bolometers of the j-th array n by using the coordinate system $\{x_j, y_j, z_j\}$, whose axis Oy_j coincides with that of the central wire. Let us assume that axis Oy_j is rotated by angle θ_j with respect to axis O_y. Keeping in mind the short length of the laser pulse compared to the thermal constant time of the bolometer, one may assume that variation of bolometer resistance ΔR will be determined by the integral of power by the pulse time or by the energy distribution of the laser pulse $P(x, y, z)\big|_{z=z'}$.

$$\Delta R = \gamma \int_{-\infty}^{\infty} P[x(x_j, y_j),\ y(x_j, y_j)]\,dy_j, \qquad (1)$$

where γ is the absorption coefficient dependent on the wire diameter, the material from which it is made and in the general case on the polarization of the incident radiation. Graphs of the dependence $k \sim \gamma/d$ on λ provided that $d \gg \lambda$ for cylinders of various metals and for two polarizations of incident radiation with respect to the cylinder axes are presented in Figure 2, taken from [4].

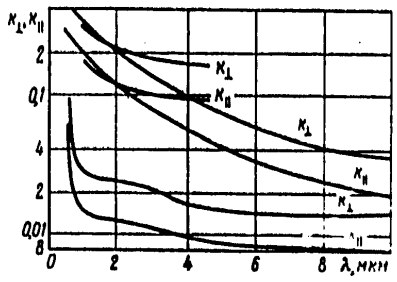

Figure 2. Dependence Of Coefficients Of Absorption Of Electromagnetic Radiation $k_{\parallel}$, $k_{\perp}$ By Cylinders Of Different Metals On Wavelength. The first two curves (from top to bottom) -- Pt; the second two curves -- Ni; the last two curves -- Au

If the measured voltage or current increment on the i-th bolometer of the j-th array is denoted by $g(x^i_j)$, the signals of all bolometers of the array determine the sequence $\{g(x^i_j)\}$, each term of which is related to energy distribution P (x, y) by the relation

$$g(x_j') = \alpha \int_{-\infty}^{\infty} P[x(x_j, y_j), y(x_j, y_j)]\delta(x_j')\,dx_j\,dy_j. \qquad (2)$$

Coefficient α depends on the absorption coefficient γ. The sequence $\{g(x^i_j)\}$ determines the discrete projection of the desired distribution function P (x, y) onto axis Oy_j. With this approach, the problem of measuring the energy distribution reduces to that of restoring the function of two variables P (x, y) by discrete projections measured at angles θ_j. Radon [5], who used a method similar to iterative methods, was apparently the first to work successfully on the problem of restoring the functions of several variables by their projections. In the considered case an approach based on the mathematical apparatus of Fourier transformations (PF) of functions of many variables is more promising.

Two important properties related to projection of function f (x) with the Fourier-image of this function are subsequently required. The first property consists in the fact that if f (x) and F (ω) form the pair PF, then F (xA) and F (ωA) will also be the pair PF provided that matrix A, which describes the transformation of coordinates, is orthogonal. The second property, also called the theorem on projections and cross-sections [6], permits one to state that (N-1)-dimensional PF of projection is the cross-section of the N-dimensional PF of function f (x). Taking both properties into account, one may conclude that the projection for which the projection axis is the transformed coordinate axis u_j, has (N-1)-dimensional PF, which is the cross-section F (Ω) at $\Omega_j = 0$, and coordinate systems u and Ω are related to systems x and ω by the same orthogonal transformation

$$x=uA, \quad \omega=\Omega A. \tag{3}$$

In the considered case, rotation of each bolometer grid around axis Oz by angle θ_j is described by orthogonal transformation of coordinates

$$A=\begin{bmatrix} \cos\theta_j & \sin\theta_j \\ -\sin\theta_j & \cos\theta_j \end{bmatrix}. \tag{4}$$

In this regard the data obtained from each bolometer array and which determined the discrete projection of distribution P (x, y) at angle θ_j simultaneously determine the cross-section of the Fourier-image of spectral distribution at the same angle and space. The relationship between the projections of the function of two variables and the cross-section of its PF is presented in Figure 3.

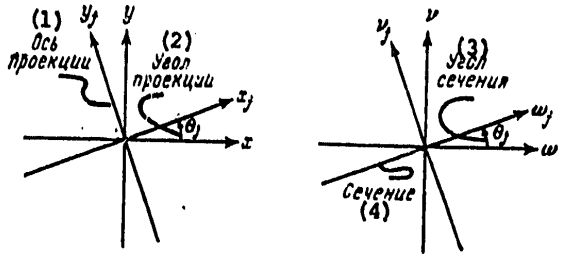

Figure 3. Relationship Between Projection Of Two-Dimensional Function And Cross-Section Of Its Fourier Transform

KEY:

1. Projection axis
2. Angle of projection
3. Angle of cross-section
4. Cross-section

By using the properties of PF pairs outlined above, one can construct the algorithm for restoration of energy distribution P (x, y) by the measured sequences (2). The main steps will be the following.

1. Measuring the oriented arrays of sequences (2) in the appropriate manner by using M.

2. Determining the images oriented in space according to orientation of the signal arrays in space by using the discrete Fourier transform (DPF) M of the Fourier-image cross-sections of the desired distribution (P) x, y.

3. Applying the images of the effective interpolation operation obtained by readings in space to find the array of readings required for reverse DPF.

4. Calculating the readings of the desired two-dimensional function P (x, y) in the signal space by applying the two-dimensional reverse DPF to the readings in the spectral space.

5. Interpolation of the derived readings to determine the values of the desired function P (x, y).

It should be noted in conclusion that machine realization of the described process of restoration can be based on use of the "fast PF" algorithm [7], which significantly reduces the losses of machine time. Moreover, the discrete nature of measuring the projections by using bolometers permits efficient organization of data input into the computer.

BIBLIOGRAPHY

1. Bautin, A. V., Yu. A. Polyakov and A. A. Shilyayev, KVANTOVAYA ELEKTRONIKA, Vol 3, 1976.

2. Konozenko I. D., ZHTF, Vol 20, 1950.

3. Kuz'michev, V. M. and A. B. Katrich, KVANTOVAYA ELEKTRONIKA, Vol 2, 1975.

4. Kuz'michev, V. M., Yu. M. Latynin and I. A. Priz, PRIBORY I TEKHNIKA EKSPERIMENTA, Vol 2, 1974.

5. Radon, J., BERICHTE VERHANDL. SACHS. GESELLSCHAFT. MATH.-PHYS. KL., Vol 69, 1917.

6. Mersero, R. and A. Oppenkheym, TIIER, Vol 62, No 10, 1974.

7. Cooly, J. W. and J. W. Tukey, MATH. COMPUT., Vol 19, 1965.

6521
CSO:8144/0823

PUBLICATIONS

NEW PUBLICATION REVIEWS LATEST GEOPHYSICAL INSTRUMENTS, APPLICATIONS

Leningrad GEOFIZICHESKAYA APPARATURA (Geophysical Equipment) in Russian Issue 64, 1978 signed to press 24 Mar 78 pp 187-189

[Table of contents from collection of articles, Izdatel'stvo Nedra, 1,900 copies, 192 pages]

[Text] Table of Contents

Electrometry

Nuclear Geophysics

Well Geophysics

11,176
CSO: 1870

END